Adjoint Based Control and Optimization of Aerodynamic Flows

by

Mattias Chevalier

June 2002
Technical Reports from
Royal Institute of Technology
Department of Mechanics
SE-100 44 Stockholm, Sweden

Typsatt i $\mathcal{AMS}$-LaTeX.

Akademisk avhandling som med tillstånd av Kungliga Tekniska Högskolan i Stockholm framlägges till offentlig granskning för avläggande av teknologie licentiatexamen onsdagen den 5:te juni 2002 kl 10.15 i sal E3, Huvudbyggnaden, Kungliga Tekniska Högskolan, Osqars Backe 14, Stockholm.

Edita Norstedts Tryckeri AB, Stockholm 2002

In memory of Nils

Adjoint Based Control and Optimization of Aerodynamic Flows

Mattias Chevalier
Department of Mechanics, Royal Institute of Technology
S-100 44 Stockholm, Sweden

Abstract

Adjoint based optimal controls both for transitional boundary flows and for quasi-1D Euler flow are studied in this thesis. A nonlinear optimization problem governed by the Navier–Stokes equations is solved using the associated adjoint equations to minimize the objective function measuring the energy of the perturbation to a laminar flow. The optimization problem is derived and implemented in the context of direct numerical simulations of incompressible spatially-developing three-dimensional boundary layer flows and the gradient computation is verified with finite-differences. The nonlinear optimal control is shown to be more efficient in reducing the disturbance energy than an optimal control based on the Orr–Sommmerfeld–Squire equations when nonlinear interactions are becoming significant in the boundary layer. For weaker disturbances the two methods are quite similar. Tollmien-Schlichting waves, streamwise streaks, and cross-flow vortices have all been controlled successfully with a nonlinear control.

The same adjoint based solution strategy is applied to another optimization problem which is governed by the quasi-1D Euler equations and where we want to find the optimal shape of a nozzle. The impact of the choice of boundary conditions and discretization of the problem on the convergence rate of the optimization algorithm is studied. Numerical experiments at subsonic and transonic speeds, show that the gradient evaluations are accurate enough to obtain satisfactory convergence of the quasi-Newton algorithm.

Descriptors: transition control, flow control, nonlinear optimal control, boundary layer flow, Falkner–Skan–Cooke flow, quasi-1D flow, shape optimization, adjoint equations, DNS

Preface

This thesis deals with adjoint based optimization methods applied to different aerodynamic flows and configurations. The thesis is divided in two parts, the first part is a short introduction to the adjoint based methodology applied to optimal control problems and the second part contains the papers. A guide to the papers and the contributions of different authors is included in the last chapter of the thesis.

The three papers in part two are adjusted to comply with the present thesis format for consistency, but their content have not been altered compared to published versions except for minor corrections.

Stockholm 2002-05-06
Mattias Chevalier

Contents

Part 1

Summary

CHAPTER 1

Introduction

The interest in controlling complex physical phenomena has grown as the need for and the possible benefits from this knowledge have become clearer, both economically but also environmentally. The field of aerodynamics is no exception. For example, large amounts of money could be saved if one could lower the fuel consumption of an airplane by just a fraction. Controlling the flow around the aircraft might be one way to achieve that.

Interest in different aspects of flow control goes back hundreds of years and this interest has now grown into a well-established research area. The notion of flow control includes a wide variety of both methods and applications and a classification of those methods is useful. The first distinction is whether energy is fed into the flow or not. In *passive* control methods the flow field is altered without any energy addition. For example by putting small pieces of metal on a wing, so called vortex generators, the flow field around the aircraft can be slightly altered in a way that reduces drag. Another classical example is the golf ball that would fly shorter if it had no dimples. The dimples trigger turbulence which in turn delay separation and drag is reduced. In *active* control methods, an energy input to the flow is required. This can be done in two ways, either in a predetermined manner, open loop, or in a closed loop form, where some measurements are input to the control loop. The latter method is also known as *reactive control*, which emanates from the fact that measurements of the state is fed back to the controller that *reacts* on the basis of that information.

A few recent review articles of both experimental and numerical efforts on the subject can be found in Bushnell & McGinley (1989), Metcalfe (1994), Moin & Bewley (1994), Joslin *et al.* (1996), Gad-el-Hak (1996), Bewley *et al.* (1997), Lumley & Blossey (1998). More mathematical aspects of optimization methods for flow control can be found in the books edited by Gunzburger (1995) and Sritharan (1998).

During the last decade, new approaches to solve flow control problems have emerged. By formulating the flow control problems as optimization problems where one wants to minimize or maximize some flow properties, one obtains a problem similar to what is studied in *optimal control* theory. The early publications regarding optimal flow control problems, such as Abergel & Temam (1990), Glowinski (1991), Gunzburger *et al.* (1989), Sritharan (1991*a*), Sritharan (1991*b*), and Gunzburger *et al.* (1992) are mostly concerned with theoretical aspects of the optimal control problem. Once the theoretical foundation

was built, subsequent publications present results from numerical simulations where the optimal control for different flow configurations is computed. One such publication is Joslin *et al.* (1997) where the optimal control of spatially growing two-dimensional disturbances in a boundary layer over a flat plate is computed. In Berggren (1998) the vorticity is minimized in an internal unsteady flow using blowing and suction on a part of the boundary and in He *et al.* (2000) two different control approaches are tested to reduce the drag resulting from the flow around a cylinder. The first approach is to use cylinder rotations to control the flow and the other is to use blowing and suction on parts of the cylinder wall. In Pralits *et al.* (2002) convectively unstable disturbances are controlled. This is done by computing the optimal wall normal velocity distribution on the wall of a steady meanflow for a given disturbance.

A recent review of computational efforts in flow control is given in Hinze & Kunish (2000), and e.g. Bewley (2001) and Högberg (2001) give overviews of different flow control approaches.

In e.g. Jameson (1989) and Jameson (1995), better aerodynamic properties of wings and air foils are computed by formulating the governing equations of the physics and the restrictions on the geometry as a *shape optimization* problem. This may be viewed as a flow-control problem in which the geometry is the control variable. The possibility to solve the problem in an automated fashion is a big improvement over a trial and error approach. In addition, repeated trials give no guarantees at all whether a truly optimal design will be found or not.

When the number of parameters to optimize are small, *direct search methods* such as genetic algorithms can be used, but when having many degrees of freedom of the control, gradient based optimization algorithms are usually much more efficient. The gradient information can be computed in many different ways but with many parameters to find in the optimization problem, the most tractable approach is to solve the *adjoint equations* associated with the equations modeling the physics. From the solution of the adjoint equations, we obtain information about where the process is most sensitive to small modifications in the control. That information can also be used to compute the gradient in a procedure that is independent of the dimensionality of the optimization problem.

The application of adjoint based methods to various optimization problems within the field of aerodynamics plays a central role in all included papers. However, the main effort has been to develop tools to be able to make sensitivity computations in three-dimensional boundary layer flows in order to find the optimal control for the flow configurations under consideration. Paper 1 and paper 2 contain the present status of that effort. Paper 3 contains a smaller study of discretization issues and choice of boundary conditions and their effect on the accuracy of the gradient. These issues are studied in the context of a quasi-1D nozzle.

CHAPTER 2

Optimal control

2.1. Introduction

The goal of an optimal control problem is to minimize or maximize an objective function. When formulating such a problem, three important issues need to be settled:

- the choice of governing equation (state equation),
- how to control the flow,
- what properties of the flow to control.

For a particular flow geometry with given fluid properties, each choice has to be made with care. The state equation should of course model the appropriate physics. This choice also indirectly affect the choice of methods to use when solving the optimal control problem. If we are working with nonlinear governing equations, such as the Navier–Stokes equations, we have to use an iterative procedure to solve the optimization problem and retrieve the optimal control, whereas when working with linear governing equations the optimal control can be computed in one step.

A governing dynamical system can be written on the general form

$$\frac{\partial x}{\partial t} = \mathcal{A}(x) + \mathcal{B}(x, \varphi), \quad x(t = 0) = x_0, \tag{2.1}$$

where x denotes the state variable, the operator $\mathcal{A}$ includes the dynamics of the model, and operator $\mathcal{B}$ describes how the control φ forces the system. There are numerous ways to affect and control the flow in an efficient way. Injection and suction of fluid through small holes or distributed over an area is one already mentioned method. Other means of control are, for example, heating and cooling and geometry changes. If the fluid is conductive, one can also use electric and magnetic fields to affect the flow.

To get the desired effect out of the control one needs to choose what properties of the flow to target. This choice is formulated as an *objective function*

$$J = \frac{1}{2} \int_0^T (x^* \mathcal{S}^* \mathcal{S} x + \varepsilon \varphi^* \varphi) \, \mathrm{d}t \tag{2.2}$$

where S is an operator measuring the quantity to be minimized in the flow, the superscript * denotes the complex conjugate transpose, and $(0, T)$ is the time interval. A regularization term with the parameter ε is also added to put a limit

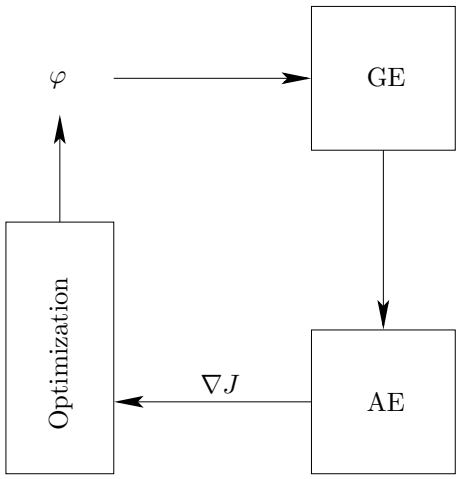

FIGURE 2.1. The optimization procedure. The control is denoted φ. The gradient of the objective function with respect to the control φ is denoted ∇J where J is the objective function. The governing equations and associated adjoint equations are denoted GE and AE respectively.

on the control. The choice of objective function is usually a non-trivial matter due to the complicated physics present in aerodynamic flows. In paper 1 and paper 2 the objective functions measure the flow perturbation energy over an *observation interval* in time and space and the spatial extent is not restricted to the wall surface but allowed to extend in the wall normal direction into the flow field. In paper 3, where an optimal shape is sought, the error norm between a desired pressure distribution and the actual pressure distribution is measured.

2.2. Nonlinear optimization

We can now formulate the nonlinear optimization problem as: find $\varphi = \varphi_{\text{opt}}$ such that $J(\varphi_{\text{opt}}) \leq J(\varphi)$ for all φ belonging to the set of admissible controls. As mentioned the non-linearity in the state equation prohibits direct solution of the nonlinear optimization problem. Instead an iterative procedure is needed to find the optimal control. The general procedure is described in Figure 2.1. First, the governing equations (GE) are solved with an initial guess of φ. From the solution of the governing equations one can solve the corresponding adjoint equations (AE). Once the state and adjoint state are solved, we can construct the gradient of the objective function with respect to the control. We can then update the control with, for example, a conjugate gradient method or a quasi-Newton method. The whole loop is repeated until a satisfactory control is found.

The drawback with this kind of control is that it will only work under exactly the very conditions the control is constructed for. On the other hand, no

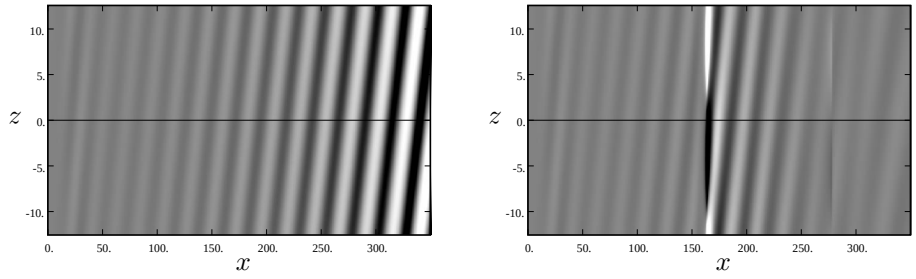

FIGURE 2.2. Snapshot of the wall normal velocity component in an xz-plane at $y = 0.5$ without control (left) and with nonlinear control (right). The control is applied in $x \in (145, 295)$. The black to white scale lies in the interval $v \in (-0.001, 0.001)$.

a priori knowledge of the control is needed, and the performance obtained with the nonlinear optimization procedure often far exceeds the result from other simplified control finding approaches. One obvious application is to determine an upper limit of what is possible to achieve with a certain control scheme, something that might aid in the search for more efficient direct methods of control.

An example of nonlinear optimal control in action is shown in Figure 2.2 where cross-flow vortices in a Falkner–Skan–Cooke boundary layer are developing downstream. In the left plot the flow is uncontrolled whereas the nonlinear optimal control is active in the right plot. The results are taken from simulations in paper 1.

2.2.1. *The gradient*

To derive a gradient expression of the objective function with respect to the control φ, we differentiate equation (2.2),

$$\delta J = \int_0^T x^* \mathcal{S}^* \mathcal{S} \delta x + \varepsilon \varphi^* \delta\varphi \, \mathrm{d}t \triangleq \int_0^T \left(\frac{\partial J}{\partial \varphi} \right)^* \delta\varphi \, \mathrm{d}t, \tag{2.3}$$

and the state equation (2.1),

$$\frac{\partial \delta x}{\partial t} - \Big[\nabla_x \mathcal{A}(x) + \nabla_x \mathcal{B}(x, \varphi) \Big] \delta x = \nabla_\varphi \mathcal{B}(x, \varphi) \delta\varphi, \quad \delta x(t = 0) = 0. \tag{2.4}$$

where

$$\nabla_x \mathcal{A}(x) = \frac{\partial \mathcal{A}(x)}{\partial x}, \quad \nabla_x \mathcal{B}(x, \varphi) = \frac{\partial \mathcal{B}(x, \varphi)}{\partial x}, \quad \text{and} \quad \nabla_\varphi \mathcal{B}(x, \varphi) = \frac{\partial \mathcal{B}(x, \varphi)}{\partial \varphi}.$$

Then by defining the inner product $\langle \cdot, \cdot \rangle$ as

$$\langle p, \delta x \rangle = \int_0^T p^* \delta x \, \mathrm{d}t, \tag{2.5}$$

and using the adjoint identity,

$$\langle p, \mathcal{N} \delta x \rangle = \langle \mathcal{N}^\star p, \delta x \rangle + \text{boundary terms}, \tag{2.6}$$

where $\mathcal{N}$ is a differential operator, we can define the adjoint of the state equation

$$-\frac{\partial p}{\partial t} - \left[\nabla_x \mathcal{A}(x) + \nabla_x \mathcal{B}(x, \varphi) \right]^\star p = \mathcal{S}^* \mathcal{S} x, \quad p(t = T) = 0. \tag{2.7}$$

Inserting the adjoint equation into the differentiated objective function yields an expression for the gradient

$$\frac{\partial J}{\partial \varphi} = \left[\nabla_u \mathcal{B}(x, \varphi) \right]^\star + \varepsilon \varphi. \tag{2.8}$$

The derivation of the adjoint equations and the gradient expression in paper 2 follows the outline given above.

2.2.2. *Computational issues*

The computational effort to solve the adjoint state is comparable to the solution of the state equation. Thus, the gradient can be determined by roughly the computational cost of solving two state equations, this cost being and independent of the number of degrees of freedom of the control parameterization. Note that the adjoint equations are always linear equations.

For unsteady simulations where the temporal history of the state equation is needed in the adjoint state computation the storage requirement can be very large. However, this requirement can be lowered using a *checkpointing technique*, see e.g. Berggren (1998). The price for the decreased storage demand is increased execution time. A memory reduction from N to $\sqrt{N}$, increases the computational cost with about a factor two.

Another important issue when deriving the discrete adjoint equations to be solved numerically is in what order the discretization takes place. One way is to discretize the expressions for the adjoint equations and the gradient that have been derived on the "continuous" level. An alternative is to discretize the Navier–Stokes equations and the objective function and *derive* the adjoint equations and the gradient expression on the discrete level. The latter approach leads to more accurate gradient directions, but it seems difficult to apply for the present discretizations. Issues related to the errors introduced by the approximative (continuous) formulation are discussed in e.g. Glowinski & He (1998) and Gunzburger (1998). The use of the continuous formulation is motivated by the findings in Högberg & Berggren (2000) where one conclusion

is that it is sufficient to use the approximative (continuous) formulation in order to control strong instabilities. It was noted that in such cases, most of the reduction of the objective function is achieved in the first few iterations, and additional iterations only result in a fine tuning of the control. The drawback is that it will require more iterations to reach the true optimal solution, if it is even possible, than with the discrete formulation. In paper 1 and paper 2 a continuous derivation of the gradient is performed whereas in paper 3 a discrete gradient is derived, except for the artificial viscosity term which is not taken into account at all.

2.3. Linear optimization

If we assume that the operators $\mathcal{A}$ and $\mathcal{B}$ in equation (2.1) are linear, the optimization problem can be solved with a direct method, since we immediately can identify the solution from the equations and solve it numerically. With these assumptions, the governing equation can be written as

$$\frac{\partial x}{\partial t} = \mathcal{A}x + \mathcal{B}\varphi, \quad x(t=0) = x_0, \tag{2.9}$$

and the gradient expression becomes

$$\frac{\partial J}{\partial \varphi} = \mathcal{B}^\star p + \varepsilon\varphi, \tag{2.10}$$

where again p denotes the adjoint state. If we now introduce a linear mapping such that,

$$p = \mathcal{X}(t)x, \tag{2.11}$$

where $\mathcal{X}$ is self-adjoint and non-negative, we can find the optimal solution by setting the gradient to zero which gives

$$\varphi = -\frac{1}{\varepsilon}\mathcal{B}^\star\mathcal{X}(t). \tag{2.12}$$

This is a feedback law for the control φ and by substituting the feedback law and the linear mapping into the adjoint equation and combining it with the state equation, we arrive at the operator Riccati equation for $\mathcal{X}$

$$\left(\frac{\partial \mathcal{X}}{\partial t} + \mathcal{A}^\star\mathcal{X} + \mathcal{X}\mathcal{A} - \frac{1}{\varepsilon}\mathcal{X}\mathcal{B}\mathcal{B}^\star\mathcal{X} + \mathcal{S}^*\mathcal{S}\right)x = 0, \quad \forall x, \quad X(t=T) = 0. \tag{2.13}$$

If we let $T \to \infty$ we solve for the stationary solution to the Riccati equation to get the optimal time-independent feedback law. Note that linear feedback law is the same regardless of what kind of disturbances that are present in the flow and is thus computed once and for all for a certain base flow. However, in the present work we are focusing on the situation where the governing equations are nonlinear. See Högberg & Henningson (2001) for a more thorough derivation of the linear feedback law and applications of it. For mathematical details about the Riccati equation see e.g. Ito & Morris (1998). The feedback law used in paper 1 follows the steps outlined above.

CHAPTER 3

Conclusion and outlook

In the present work, different applications of adjoint based optimization techniques of nonlinear governing systems have been investigated.

A quasi-discrete form of the adjoint equations is derived for quasi-1D Euler equations, with physically relevant boundary conditions for nozzle flow. This was done in order to be able to solve an optimization problem where the difference between the actual pressure distribution and a target pressure distribution was minimized. The gradient computation is shown to work well for subsonic and transonic flows and the optimal shape for the corresponding target pressure distributions is found.

We have implemented an adjoint solver to an already existing spectral code (Lundbladh *et al.* (1999)) that solves the incompressible Navier–Stokes equations for boundary layer flows where control is applied through blowing and suction on part of the wall, and where the objective function measures the deviation in velocity between the flow field and a laminar flow field. The adjoint code is verified with a gradient computed with finite differences of the objective function. The nonlinear control is computed and compared with the linear optimal control, see Högberg & Henningson (2001).

Some conclusions that can be drawn so far from this project are:

- Tollmien-Schlichting waves, streamwise streaks, and cross-flow vortices have all been controlled successfully with a nonlinear control.
- For weak disturbances the linear and nonlinear optimal control are quite similar.
- For flows with nonlinear interactions the nonlinear control works better than the linear control.

A natural continuation for the adjoint based control scheme is to investigate the use of other, more efficient, inner products. This choice could have a large impact on the convergence rate of the iterative process and also on how well the "optimal control" will work, see e.g. Protas & Bewley (2002). The choice of inner products is important for both shape optimization and flow control problems.

There are many other interesting flow situations, not studied here, where the nonlinear optimal control could be of interest to compute such as in a flow with a separation bubble where nonlinear interactions and nonparallel effects are pronounced.

CHAPTER 4

Quick guide to papers and authors contributions

Paper 1

Linear and nonlinear optimal control in spatial boundary layer

M. Chevalier (MC), M. Högberg (MH), M. Berggren (MB) & D. S. Henningson(DH)

A linear and a nonlinear optimal control approach are compared when applied to a spatially-developing three-dimensional boundary layer flow. The control is tested for three fundamentally different disturbance types. The flow is controlled through blowing and suction on part of the wall. Implementations and simulations have been performed by MC and MH. The report was written by MC and MH with feedback from MB and DH. Published as an AIAA paper at the 3rd Theoretical Fluid Mechanics Meeting, St. Louis, MO (AIAA 2002-2755).

Paper 2

Optimal control in wall bounded flows

M. Högberg, M. Chevalier, M. Berggren & D. S. Henningson

In this paper a solver for the nonlinear optimization problem, using the adjoint equations for gradient computations, is developed and tested for both channel and boundary layer flow. The channel flow problem has been explored by MH and the extension to boundary layer flow was performed by MC. Derivations of the adjoint equations and the gradient expressions were done by MH and MC in close cooperation with MB. Implementation for solving the channel flow problem was performed by MH and for the boundary layer flow by MC. The report was written jointly by MH and MC with feedback from MB and DH. The results presented for the channel flow case were previously published in the proceedings of ETC8, Barcelona (Högberg & Berggren (2000)). Published as a technical report at the Swedish Defence Research Agency (FOI-R--0182--SE), 2001.

Paper 3

Accuracy of gradient computations for aerodynamic shape optimization problems

M. Chevalier & M. Berggren

A gradient based optimization method is applied on an aerodynamic shape optimization problem. Issues regarding discretization and choice of boundary conditions and their effect on the accuracy of the gradient are studied. The problem formulation and theory was jointly derived by both authors. Simulations were performed by MC and the report was written by MC and MB. Much of the work was done for the MSc of MC (Chevalier (1999)), but postprocessing of data and additional simulations as well as the writing of the conference proceeding were a part of the doctoral studies of MC. Published as a proceeding to ICAS 2000 (ICA0245). A more detailed version is published as a technical report at the Swedish Defence Research Agency (at the time Aeronautical Research Institute of Sweden, FFA), Chevalier & Berggren (2000).

The papers are re-set to the present thesis format.

Acknowledgment

First of all I would like to thank my advisor Professor Dan Henningson for giving me the opportunity to work in the realm of fluid mechanics and also for generously sharing his knowledge.

I also want to thank my assistant advisor Doctor Martin Berggren for invaluable help in everything from mathematics to type setting of reports.

Many thanks to my colleagues at the Department of Computational Aerodynamics at FOI and the Department of Mechanics for providing a nice environment to work in. In particular I would like to thank Markus Högberg for patiently answering questions and always giving a helping hand when problems showed up.

Finally I want to thank my family and my friends for supporting me during my studies.

This work has been funded by the Swedish Defence Research Agency (FFA/FOI) and the Swedish Defence Materiel Administration (FMV).

Tack Anna, för din omtanke, ditt stöd och all din kärlek.

Bibliography

Abergel, F. & Temam, R. 1990 On some control problems in fluid mechanics. *Theoret. Comput. Fluid Dyn.* **1**, 303–325.

Berggren, M. 1998 Numerical solution of a flow-control problem: vorticity reduction by dynamic boundary action. *SIAM J. Sci. Comp.* **19** (3), 829–860.

Bewley, T. R. 2001 Flow control: New challenges for a new renaissance. *Prog. Aero. Sci.* **37**, 21–58.

Bewley, T. R., Moin, P. & Temam, R. 1997 Optimal and robust approaches for linear and nonlinear regulation problems in fluid mechanics (97–1872).

Bushnell, D. M. & McGinley, C. B. 1989 Turbulence control in wall flows. *Annual Rev. Fluid Mechanics* **21**, 1–20.

Chevalier, M. 1999 Drag reduction for flow past a circular cylinder using blowing and suction. Research Report UH/MD. Department of Mathematics, University of Houston, Houston, TX 77204-3476.

Chevalier, M. & Berggren, M. 2000 Accuracy of gradient computations for aerodynamic shape optimization problems. *Tech. Rep.* TN 2000-31. FFA, the Aeronautical Research Institute of Sweden, P. O. Box 11021, S-161 11 Bromma, Sweden.

Gad-el-Hak, M. 1996 Modern developments in flow control. *Appl. Mech. Rev.* **49** (7), 364–379.

Glowinski, R. 1991 *Finite element methods for the numerical solution of incompressible viscous flow. Introduction to the control of the Navier–Stokes equations*, pp. 219–301. *Lectures in Appl. Math.* 28. American Mathematical Society, Providence, RI.

Glowinski, R. & He, J. 1998 On shape optimization and related issues. In *Computational Methods for Optimal Design and Control* (eds. J. Borggaard, J. Burns, E. Cliff & S. Schreck), pp. 151–179. Birkhäuser, Boston.

Gunzburger, M., Hou, L.-S. & Svobodny, T. P. 1989 Numerical approximation of optimal control problem associated with the navier–stokes equations. *Appl. Math. Lett.* **2**, 29–31.

Gunzburger, M., Hou, L.-S. & Svobodny, T. P. 1992 Boundary velocity control in incompressible flow with an application to viscous drag reduction. *SIAM J. Control Optim.* **30**, 167–181.

Gunzburger, M. D., ed. 1995 *Flow Control*. Springer-Verlag.

Gunzburger, M. D. 1998 Sensitivities in computational methods for optimal

flow control. In *Computational Methods for Optimal Design and Control* (eds. J. Borggaard, J. Burns, E. Cliff & S. Schreck), pp. 197–236. Birkhäuser, Boston.

He, J.-W., Chevalier, M., Glowinski, R., Metcalfe, R., Nordlander, A. & Periaux, J. 2000 Drag reduction by active control for flow past cylinders. In *Computational mathematics driven by industrial problems (Martina Franca, 1999)*, pp. 287–363. Berlin: Springer.

Hinze, M. & Kunish, K. 2000 Three control methods for time dependent fluid flow. *Flow, Turbulence and Combustion* **65** (3/4), 273–298.

Högberg, M. 2001 Optimal Control of Boundary Layer Transition. PhD thesis, Royal Institute of Technology, Department of Mechanics, Stockholm, Sweden.

Högberg, M. & Berggren, M. 2000 Numerical investigation of different discretization approaches for optimal control. *Flow, Turbulence and Combustion* **65** (3/4), 299–320.

Högberg, M. & Henningson, D. S. 2001 Linear optimal control applied to instabilities in spatial boundary layers. *J. Fluid Mech.* Submitted.

Ito, K. & Morris, K. A. 1998 An approximative theory of solutions to operator riccati equations for $\mathcal{H}^\infty$ control. *SIAM J. Control Optim.* **36** (1), 82–99.

Jameson, A. 1989 Computational aerodynamics for aircraft design. *Science* **245**, 361–371.

Jameson, A. 1995 *Optimum aerodynamic design using control theory. Computational Fluid Dynamics Review* . American Mathematical Society, Providence, RI: John Wiley, New York.

Joslin, R. D., Erlebacher, G. & Hussaini, M. Y. 1996 Active Control of Instabilities in Laminar Boundary Layers–Overview and Concept Validation. *Journal of Fluids Engineering* **118** (3), 494–497.

Joslin, R. D., Gunzburger, M. D., Nicolaides, R. A., Erlebacher, G. & Hussaini, M. Y. 1997 A Self-contained, Automated Methodology for Optimal Flow Control Validated for Transition Delay. *AIAA Journal* **35** (5), 816–824.

Lumley, J. & Blossey, P. 1998 Control of turbulence. *Annual Rev. Fluid Mechanics* **30**, 311–327.

Lundbladh, A., Berlin, S., Skote, M., Hildings, C., Choi, J., Kim, J. & Henningson, D. S. 1999 An Efficient Spectral Method for Simulations of Incompressible Flow over a Flat Plate. Technical Report TRITA-MEK 1999:11. Royal Institute of Technology, Department of Mechanics, KTH.

Metcalfe, R. W. 1994 Boundary layer control: A brief review. In *Computational Fluid Dynamics '94, Invited Lectures of the Second European CFD Conference* (eds. S. Wagner, J. Periaux & E. Hirschel), pp. 52–60. Stuttgart, Germany: John Wiley & Sons.

Moin, P. & Bewley, T. R. 1994 Feedback control of turbulence. *Appl. Mech. Rev.* **47** (6), part 2, S3–S13.

Pralits, J., Hanifi, A. & Henningson, D. S. 2002 Adjoint-based optimization of steady suction for disturbance control of incompressible flows. *J. Fluid Mech.* Accepted.

Protas, B. & Bewley, T. R. 2002 Regularization opportunities in the adjoint analysis of multiscale systems. In *Advances in Turbulence IX* (eds. I. P. Castro, P. E. Hancock & T. G. Thomas). Proceedings of the Ninth European Turbulence Conference.

Sritharan, S. 1991*a* Dynamic programming of Navier–Stokes equations. *System Control Lett.* **16**, 299–307.

Sritharan, S. 1991*b* An optimal control problem for exterior hydrodynamics. In *Distributed Parameter Control Systems: New Trends and Applications* (eds. G. Chen, E. Lee, W. Littman & L. Markus), pp. 385–417. Marcel Dekker, New York.

Sritharan, S. S., ed. 1998 *Optimal control of viscous flows*. SIAM.

Part 2

Papers

1

Paper 1

Linear and nonlinear optimal control in spatial boundary layer

By Mattias Chevalier[†], Markus Högberg[†], Martin Berggren[†‡§] and Dan S. Henningson[*†]

Instabilities in a spatially-developing three-dimensional boundary layers are controlled through blowing and suction at the wall. The performance of the control is tested in direct numerical simulations (DNS) of the incompressible Navier–Stokes equations for Tollmien–Schlichting (TS) waves, optimal transiently growing streaks in a Blasius boundary layer, and cross flow vortices in a Falkner–Skan–Cooke (FSC) flow. Two control strategies are compared.

First, a quasi-Newton optimization algorithm is applied to solve an off-line optimal control problem. A solver for the adjoint equations has been implemented in the spectral DNS code used. This method adapts naturally, without modification, to nonlinearities such as a strongly varying mean flow. However, it is computationally expensive and storage demanding, needing numerous solves of the Navier–Stokes and associated adjoint equations.

Second, feed-back optimal control is applied, using a strategy designed to operate locally on a spatially-developing flow. The feed-back operator is constructed from the Orr–Sommerfeld–Squire equations. Assuming the flow to be locally parallel makes it feasible to solve the associated Riccati equations for each wave number pair in the stream- and spanwise directions. The feed-back is applied to a DNS of the flows mentioned above. This method is much less computationally costly than the first nonlinear method. The method performs surprisingly well, in spite of the limitations with respect to being able to account for strong nonlinear effects. It is demonstrated that TS waves are stabilized and that transient growth is considerably lowered by the controller. Moreover, the controller successfully inhibits growth of steady cross flow vortices in the FSC flow.

1. Introduction

In flow systems where strong inherent instabilities are present, like in a transitional boundary layer flow, small perturbations can alter the flow features

[*]Department of Mechanics, Royal Institute of Technology (KTH), SE-100 44 Stockholm, Sweden
[†]The Swedish Defence Research Agency (FOI), SE-172 90 Stockholm, Sweden
[‡]Department of Scientific Computing, Uppsala University
[§]Presently, Sandia National Laboratories, PO Box 5800, Albuquerque, NM 87185, USA

dramatically. In such flows, there is therefore a potential to improve the quality of the flow using small devices with a localized action and with a minimum of energy expenditure. This is one of the main ideas behind flow control. Such control strategies could be used, for example, to reduce drag on bodies, increase lift on wings, increase propulsion efficiency, heat- and mass-transfer reduction or enhancement, control of vortex shedding or to control separation and aeroacoustic pressure fluctuations.

Generally, the different control techniques are divided into two groups. The first group, where no auxiliary power is used, includes the passive control methods. These methods are usually implemented through geometrical modifications. This has been the traditional way of controlling fluid mechanical systems. The other large group of control methods is the active control methods where the control is adjusted dynamically to the state of the system. This is what most of the work on control today is focused on. One of the first attempts was, for example, to cancel TS waves by anti-phase modal suppression to prevent transition. Early work is reviewed in Thomas (1990) and a brief, later review is given in Metcalfe (1994). These efforts showed that instabilities may indeed be significantly suppressed, but complete elimination of the primary instability is not achieved.

As opposed to earlier attempts of controlling fluid flows, when thorough understanding of the phenomena involved was necessary, optimal control theory requires no *a priori* knowledge about the functional behavior of an effective control. The theoretical framework is general and applies to a broad spectra of applications where just a small selection is listed here: finding optimal shape of wings under certain conditions (Jameson (1989)), minimizing the vorticity of an unsteady internal flow by manipulating the inlets (Berggren (1995)), as well as controlling boundary layer transition (Joslin *et al.* (1997)) and turbulence (Bewley *et al.* (2001)). Optimal control based on linear theory has also been investigated and has shown to work very well in recent applications such as in channel flow (Joshi *et al.* (1997), Bewley & Liu (1998) and Högberg & Bewley (2001)). In this approach modern linear control theory is used to construct feedback control laws for online control.

In this paper both the linear control approach from Högberg & Bewley (2001) and Högberg & Henningson (2001) and the nonlinear control approach from Högberg *et al.* (2001) are applied to spatially evolving boundary layer flows in cases representing three fundamentally different paths to transition. Our goal is to measure the effectiveness of the optimal nonlinear controller versus the linear counterpart and how much the restrictions in the linear optimal control limits its performance. Note however that the two optimization formulations differ in terms of objective functions. See text below for details.

In section 2 the two optimization problem formulations are briefly explained, and a short description of the numerical methods used are described

in section 3. In section 4 the two control approaches are applied to three different flow scenarios and results from these simulations are presented. Finally, a summary and conclusions follow in section 5.

2. Problem formulations

When formulating an optimal control problem, three important issues need to be settled: the choice of state equation, how to control the flow, and what properties of the flow to control. For a particular flow geometry and with given fluid properties, these choices have to be made with care.

In this work, the governing equations are the incompressible Navier–Stokes equations for the nonlinear controller and the corresponding equations linearized around a base flow for the linear controller. Control is exerted through blowing and suction on a part of the wall. In order to limit the control effects on the mean flow, zero-mass flux is enforced on the control. Finally, we choose an objective function that gives a measure of how close the controlled flow is to a laminar flow and thus indicates how well the control is working.

Since no single quantity is known to tell where on the path to transition we are, there is no obvious choice of objective function. The mean skin friction drag could be used as an indicator, since it has a jump at transition, and can be used to define a transition point, (Reddy *et al.* (1998)). On the other hand, Bewley *et al.* (2001) showed that this is not a good choice of objective function when the purpose is to relaminarize turbulence in channel flow, and concluded that the turbulence kinetic energy was a more appropriate choice. Since we here are interested in control of transition rather than turbulence, the energy of the deviation from the laminar flow appears to be an appropriate quantity to minimize. An increased physical understanding of the transition process and the crucial mechanisms of turbulence could provide a guide to the best choice of objective function as pointed out by Kim & Lim (2000).

The computational domain, depicted in Figure 1, is

$$\begin{aligned} \Omega &= (-x_l/2, x_l/2) \times (0, y_\infty) \times (-z_l/2, z_l/2), \\ Q &= \Omega \times (0, T). \end{aligned} \tag{1}$$

We denote by Γ the boundary of the domain. The lower part ($y = 0$) of the computational box is denoted Γ_l and the upper part ($y = y_\infty$) Γ_u. In addition Γ_c represents the part of the lower boundary where control is applied. For temporal simulations Γ_c usually coincide with Γ_l.

As already mentioned, the growing boundary layer is governed by the incompressible Navier–Stokes equations

$$\begin{aligned} \frac{\partial u}{\partial t} + (u \cdot \nabla)u - \frac{1}{Re}\Delta u + \nabla \pi &= \lambda(x)(U - u) \text{ in } Q, \\ \nabla \cdot u &= 0 \quad \text{in } Q, \\ u|_{t=0} &= u_0, \end{aligned} \tag{2}$$

with periodic boundary conditions in the horizontal directions, that is, the x- and z-directions,

$$\begin{aligned} u|_{x=-x_l/2} &= u|_{x=x_l/2}, \\ u|_{z=-z_l/2} &= u|_{z=z_l/2}. \end{aligned} \tag{3}$$

The Reynolds number Re is based on the free stream velocity U_∞ and the displacement thickness δ^*, both evaluated at the streamwise location x_0. To model a pressure gradient the free-stream velocity is forced to obey

$$U_\infty = \left(\frac{x}{x_0} + 1\right)^m \tag{4}$$

where m is a parameter related to the strength of the pressure gradient. When the Reynolds number is based on the local displacement thickness and freestream velocity, the notation R is used. The pressure is denoted π. The term $\lambda(x)(U-u)$ is a forcing term used to make the flow situation sketched in Figure 1 periodic, enabling the use of Fourier discretization in simulations of the physical flow. This is known as a *fringe region* technique and is described further in Lundbladh *et al.* (1999) and analyzed by Nordström *et al.* (1999). Left to be specified are the conditions on the wall and in the free-stream. On the wall, the boundary condition for the horizontal velocities is a no-slip condition, and the wall normal velocity v_c is given by the control. The free-stream boundary condition should be applied at $y = y_{\text{fst}}$ where $y = y_{\text{fst}}$ is large enough not to be influenced by the existence of the boundary layer. However, the simulation box has to be of reasonable height. A simple artificial boundary condition located at y_∞ is thus used to allow truncation of this large domain. Here a Neumann condition is used at the artificial free-stream boundary. This choice allows a smaller height of the simulation box, compared to if the free-stream condition was enforced through a Dirichlet condition. All together, the following boundary conditions are specified:

$$\begin{aligned} u|_{y=y_{\text{fst}}} &= U_\infty, \ \left(\text{approx. by } \left.\frac{\partial u}{\partial n}\right|_{\Gamma_u} = 0\right), \\ u|_{\Gamma_c} &= n v_c, \\ u|_{\Gamma_l \setminus \Gamma_c} &= 0. \end{aligned} \tag{5}$$

We expand the control v_c in basis functions $\psi_{l,m}$ with zero mass flux, where $\varphi_{l,m}$ are time dependent coefficients for the basis functions,

$$v_c(x,z,t) = \begin{cases} \varphi_l^T \psi_l = \displaystyle\sum_{m=1}^{M} \varphi_{l,m}(t)\psi_{l,m}(x,z) & \text{in } (T_1^c, T_2^c), \\ 0 & \text{otherwise}, \end{cases} \tag{6}$$

where we have introduced the control vector φ_l defined as:

$$\varphi_l = (\varphi_{l,1}, \ldots, \varphi_{l,M})^T.$$

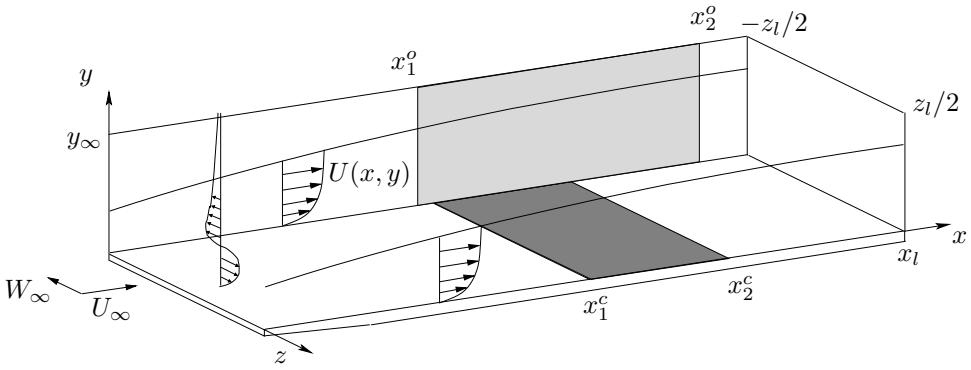

FIGURE 1. The computational domain. In the nonlinear optimization problem the flow is observed in the region $[x_1^o, x_2^o] \times [0, y_\infty] \times [-z_l/2, z_l/2] \times [T_1^o, T_2^o]$. For both optimization problems the control region is $[x_1^c, x_2^c] \times [-z_l/2, z_l/2] \times [T_1^c, T_2^c]$.

Furthermore, the control is restricted in time and allowed to be active only during the time interval $t \in (T_1^c, T_2^c)$.

2.1. *Nonlinear control*

In order to quantify the control objective, we introduce the objective function

$$J(\varphi) = \frac{\varepsilon}{2} \int_{T_1^c}^{T_2^c} \int_{\Gamma_c} |v|^2 \, \mathrm{d}\Gamma \, \mathrm{d}t + \frac{1}{2} \int_{T_1^o}^{T_2^o} \int_{\Omega_o} |u - u_T|^2 \, \mathrm{d}Q, \tag{7}$$

where the deviation energy from a given target velocity distribution u_T is minimized. Also a regularization term, including the parameter $\varepsilon > 0$, is added in order to limit the control energy itself. The control is applied over the time interval $t \in (T_1^c, T_2^c)$ and the flow is observed over space Ω_0 and over time interval $t \in (T_1^o, T_2^o)$.

The nonlinear optimization problem can now be formulated as: Find $\varphi_{\mathrm{opt}} \in \mathcal{U}_{\mathrm{ad}}$ that satisfies

$$J(\varphi_{\mathrm{opt}}) \leq \varphi \quad \forall v(\varphi)|_{\Gamma_c} \in \mathcal{U}_{\mathrm{ad}}, \tag{8}$$

where $\mathcal{U}_{\mathrm{ad}}$ denotes the set of admissible controls, which is a subset of $L^2((T_1^c, T_2^c); \mathbb{R}^M)$, and where u in objective function (7) is obtained from solving the Navier–Stokes equations (2) supplied with boundary conditions (3) and (5), in which the control is acting on the system according to expansion (6).

Due to the nonlinearities in the state equation, we solve this optimization problem using an "off-line" iterative procedure. That is, the Navier–Stokes equations solved numerous times when the optimization algorithm successively computes better and better approximations of the optimal control. In contrast,

a feedback operator can be computed once and for all in the linear case, as described in the next section, and the optimal control is then computed "on line" during a single solution of the Navier–Stokes equations. In the nonlinear case, we have chosen a gradient-based optimization algorithm and to compute the gradient of the objective function by solving the associated adjoint equations. With this approach, the cost of evaluating the gradient is independent of the number of degrees of freedom for the control, a feature that is particularly attractive for unsteady problems.

We discretize the expressions for the adjoint equations and the gradient after that they have been derived on the "continuous" level. An alternative is to discretize the Navier–Stokes equations and the objective function and derive the adjoint equations and the gradient expression on the discrete level. The latter approach leads to more accurate gradient directions, but it seems difficult to apply for the present discretizations. Issues related to the errors introduced by the approximative (continuous) formulation are discussed by e.g. Glowinski & He (1998) and Gunzburger (1995). The use of the continuous formulation for the present problem is motivated by the findings in Högberg & Berggren (2000), where one conclusion was that it is sufficient to use the approximative formulation in order to control strong instabilities. It was noted that in such cases, most of the reduction of the objective function is achieved in the first few iterations, and that additional iterations only result in a fine tuning of the control. The drawback is that more iterations are required to reach the true optimal control, if even possible, compared to the case when the gradient is derived on the discrete level.

Figure 1 presents a schematic view of the computational domain. Note that we can separate the part of the domain where we observe the flow and where we control it, both in space and time. The observation interval is chosen to be over the complete simulation time for all simulations, but the spatial extent is smaller than the complete simulation box since we want to exclude the effects from the fringe region. Also, observing the flow upstream of the control, where it can have no effect, is not pertinent.

A detailed derivation of the objective function gradient can be found in Högberg *et al.* (2001). Here only the solution procedure for the optimal control problem is stated together with the final expression.

Differentiating objective function (7), state equation (2), and boundary conditions (3) with respect to a variation of the control vector φ_l and applying

integration by parts, we can derive the adjoint equations

$$\begin{aligned} &-\frac{\partial p}{\partial t} + (\nabla u)^T p - (u \cdot \nabla) p - \frac{1}{Re}\Delta p + \lambda(x) p \\ &+\nabla \sigma = \begin{cases} u - u_T & \text{in } (T_1^o, T_2^o) \times \Omega_o \\ 0 & \text{otherwise} \end{cases} \qquad \text{in } Q, \\ &\nabla \cdot p = 0 \qquad \text{in } Q, \\ &p|_{t=T} = 0, \end{aligned} \tag{9}$$

along with the boundary conditions:

$$\begin{aligned} p|_{x=-x_l/2} &= p|_{x=x_l/2}, \\ p|_{z=-z_l/2} &= p|_{z=z_l/2}, \\ p|_{\Gamma_l} &= 0, \\ p|_{y=y_{\text{fst}}} &= 0, \quad \left(\text{approx. by} \quad \left.\frac{\partial p}{\partial n}\right|_{\Gamma_u} = 0\right), \end{aligned} \tag{10}$$

where σ is the adjoint "pressure" and p the adjoint "velocity" variable. The gradient can now be written as the M-vector

$$\frac{\partial J}{\partial \varphi_l} = \int_{\Gamma_c} \psi_l \left(\varepsilon \varphi_l^T \psi_l - \sigma\right) \mathrm{d}\Gamma. \tag{11}$$

Note that the adjoint equations are solved backwards in time and that the velocity u appears in the equations. This means that we have to store the temporal history of the velocity data from the solution of the Navier–Stokes equations.

The optimization procedure can now be summarized as follows: pick an initial guess of the control, solve the Navier–Stokes equations, solve the adjoint equations, compute the gradient of the objective function, update the control and repeat as long as the optimization problem has not converged.

The nonlinear control approach is computationally expensive and storage demanding for large simulations, even though the storage requirement can be lowered by using a *checkpointing technique*, see e.g. Berggren (1998).

2.2. *Linear control*

By applying control theory using the Navier–Stokes equations linearized around some mean flow, we can directly compute an on-line feedback law. In recent studies, such linear feedback controllers have shown to be effective for both channel and boundary layer flows.

First we assume that we are considering small disturbances so that we can divide the flow into two parts,

$$(u_1, v, w) = (U, 0, W) + (u_1', v', w') \tag{12}$$

where U and W are base flow components in the chordwise and spanwise directions, respectively and where the primed quantities denote the disturbances.

We have also introduced an approximation by adopting a parallel-flow assumption, i.e. neglegting variations in the base flow in the chordwise direction. Now we assume that the wave-like disturbances are of the form

$$v' = \hat{v}(y,t)e^{i(\alpha x+\beta z)}, \tag{13}$$

where α and β are the x and z components of the wave number vector and $\hat{}$ denotes the complex amplitude function of the corresponding velocity component. Applying these assumptions on the Navier–Stokes equations and linearizing around the base flow, we obtain a set of evolution equations for the amplitude functions of the velocity components. These can be reduced to the following set of two coupled equations, where appropriate boundary conditions have been included to allow inversion of the Laplacian ($\Delta = \mathcal{D}^2 - \alpha^2 - \beta^2$),

$$\begin{aligned}
\frac{\partial \hat{v}}{\partial t} &= \underbrace{\Delta^{-1}\Big[-i(\alpha U+\beta W)\Delta + i\alpha\mathcal{D}^2U + i\beta\mathcal{D}^2W + \frac{1}{Re}\Delta^2\Big]}_{\mathcal{L}_{OS}}\hat{v},\\
\frac{\partial \hat{\eta}}{\partial t} &= \underbrace{\left[i\alpha\mathcal{D}W - i\beta\mathcal{D}U\right]}_{\mathcal{L}_C}\hat{v} + \underbrace{\left[-i(\alpha U+\beta W) + \frac{1}{Re}\Delta\right]}_{\mathcal{L}_{SQ}}\hat{\eta},
\end{aligned} \tag{14}$$

where $\eta = i(\beta\hat{u}_1 - \alpha\hat{w})$ is the complex amplitude function of the normal vorticity. The operator $\mathcal{D}$ denotes a differentiation operator with respect to the wall normal direction. Equations (14) are referred to as the Orr–Sommerfeld and Squire equations respectively. The base flow is taken from similarity solutions for the different flow cases studied. Details of the theory can be found in i.e. Schmid & Henningson (2001). The associated boundary conditions are

$$\begin{aligned}
&\hat{v}(0,t) = \hat{\varphi}\ ,\ \mathcal{D}\hat{v}(0,t) = 0\ ,\ \hat{\eta}(0,t) = 0,\\
&\hat{v}(y,t) \to 0\ ,\ \mathcal{D}\hat{v}(y,t) \to 0\ ,\ \hat{\eta}(y,t) \to 0 \text{ as } \to\infty.
\end{aligned} \tag{15}$$

The control $\hat{\varphi}$ enters the flow as the wall-normal velocity at the lower boundary.

Since the system of equations (14) is linear, we can divide the solution into a homogeneous $(\hat{v}_h, \hat{\eta}_h)$ and an inhomogeneous $(\hat{v}_p, \hat{\eta}_p)$ solution such that

$$\underbrace{\begin{bmatrix}\hat{v}\\ \hat{\eta}\end{bmatrix}}_{\hat{x}_f} = \underbrace{\begin{bmatrix}\hat{v}_h\\ \hat{\eta}_h\end{bmatrix}}_{\hat{x}_h} + \underbrace{\begin{bmatrix}\hat{v}_p\\ \hat{\eta}_p\end{bmatrix}}_{\hat{\mathcal{Z}}}\hat{\varphi}, \tag{16}$$

where the inhomogeneous (particular) solution is such that it is the stationary solution to (14) satisfying the boundary conditions (15) with $\hat{\varphi} = 1$. The system of equations can now be written as

$$\dot{\hat{x}}_h = \mathcal{N}\hat{x}_h + \mathcal{N}\hat{\mathcal{Z}}\hat{\varphi} - \hat{\mathcal{Z}}\dot{\hat{\varphi}}, \tag{17}$$

where

$$\mathcal{N} = \begin{bmatrix}\mathcal{L}_{OS} & 0\\ \mathcal{L}_C & \mathcal{L}_{SQ}\end{bmatrix}, \tag{18}$$

with the boundary condition for the inhomogeneous system is as in (15). Note that since $\mathcal{N}\hat{\mathcal{Z}}\hat{\varphi} = 0$, we can instead use the corresponding boundary conditions for the homogeneous problem,

$$\begin{aligned} &\hat{v}(0,t) = 0\ ,\ \mathcal{D}\hat{v}(0,t) = 0\ ,\ \hat{\eta}(0,t) = 0, \\ &\hat{v}(y,t) \to 0\ ,\ \mathcal{D}\hat{v}(y,t) \to 0\ ,\ \hat{\eta}(y,t) \to 0 \text{ as } \to \infty \end{aligned} \tag{19}$$

By introducing $\hat{x} = [\hat{x}_h, \hat{\varphi}]^T$, the state equation can be described as

$$\dot{\hat{x}} = \mathcal{A}\hat{x} + \mathcal{B}\dot{\hat{\varphi}}, \tag{20}$$

where

$$\mathcal{A} = \begin{bmatrix} \mathcal{N} & 0 \\ 0 & 0 \end{bmatrix}, \quad \mathcal{B} = \begin{bmatrix} -\hat{\mathcal{Z}} \\ 1 \end{bmatrix}. \tag{21}$$

In accordance with the previous discussion regarding the choice of objective function, we use the following objective function for the linear optimal control problem

$$\hat{J}(\hat{\varphi}) = \lim_{T\to\infty} \int_0^T (\hat{x}^* \mathcal{Q}\hat{x} + l^2 \dot{\hat{\varphi}}^* \dot{\hat{\varphi}})\, \mathrm{d}t, \tag{22}$$

where $\mathcal{Q}$ is an operator such that $\hat{x}^*\mathcal{Q}\hat{x}$ measures the perturbation energy, and l is a penalizing parameter for the magnitude of control $\dot{\hat{\varphi}}$. For each wave number pair, $\mathcal{Q}$ can be written as

$$\mathcal{Q} = \begin{bmatrix} \mathcal{S} & \mathcal{S}\hat{\mathcal{Z}} \\ \hat{\mathcal{Z}}^*\mathcal{S} & \hat{\mathcal{Z}}^*\mathcal{S}\hat{\mathcal{Z}} \end{bmatrix}, \tag{23}$$

where $\mathcal{S}$ is defined as

$$\begin{aligned} \hat{x}_f^* \mathcal{S} \hat{x}_f =& \frac{1}{y_\infty} \int_0^{y_\infty} \hat{x}_f \mathcal{C}^* \mathcal{C} \hat{x}_f \, \mathrm{d}y \\ =& \frac{1}{4y_\infty k^2} \int_0^{y_\infty} \left(\frac{\partial \hat{v}}{\partial y}^* \frac{\partial \hat{v}}{\partial y} + k^2 \hat{v}^* \hat{v} + \hat{\eta}^* \hat{\eta} \right) \mathrm{d}y, \end{aligned} \tag{24}$$

with $k^2 = \alpha^2 + \beta^2$. The linear optimal control problem can now be stated: Find $\dot{\hat{\varphi}}$ that minimizes the objective function (22) subject to

$$\dot{\hat{x}} = \mathcal{A}\hat{x} + \mathcal{B}\dot{\hat{\varphi}}, \quad \hat{x}(t=0) = \hat{x}_0. \tag{25}$$

This is a standard optimal control problem, and the optimal feedback control law $\dot{\hat{\varphi}} = \hat{\mathcal{K}}\hat{x}$ can now be found through the expression

$$\hat{\mathcal{K}} = -\frac{1}{l^2}\mathcal{B}^*\hat{\mathcal{X}} \tag{26}$$

where $\hat{\mathcal{X}}$ is the non-negative self-adjoint solution to the stationary operator Riccati equation

$$\left(\hat{\mathcal{X}}\mathcal{A} + \mathcal{A}^*\hat{\mathcal{X}} - \frac{1}{l^2}\hat{\mathcal{X}}\mathcal{B}\mathcal{B}^*\hat{\mathcal{X}} + \mathcal{C}^*\mathcal{C}\right)\hat{x} = 0, \quad \forall \hat{x}. \tag{27}$$

Note that since the time horizon for the objective function is infinite we seek the stationary solution to the Riccati equation and get a time independent feed back law. Applying this feedback control gives us the closed loop system

$$\dot{\hat{x}} = \underbrace{(\mathcal{A} + \mathcal{B}\hat{\mathcal{K}})}_{\mathcal{A}_{\rm cl}}\hat{x}, \tag{28}$$

where $\mathcal{A}_{\rm cl}$ describes the dynamics of the controlled system. More details on the derivation can be found in Högberg & Henningson (2001). For details on this type of optimal control theory the reader is referred to e.g. Ito & Morris (1998) and Hulsing (1999).

The control problem is solved for an array of wave number pairs, corresponding to a sufficient resolution for the flow of interest, and the resulting controllers are combined into a physical space controller through an inverse Fourier transform. The feedback law is then represented as a convolution of this physical space control law and the velocity field.

The limitations of this approach are mainly that nonlinear as well as non-parallel effects are neglected. The optimization is performed over an infinite time horizon, and thus no guarantees can be made regarding instantaneous behavior and initial transients.

3. Implementation

A pseudo-spectral method is used to solve the incompressible Navier–Stokes equations for flow over a flat plate with or without an external pressure gradient. Fourier-series expansions are used in the chordwise and spanwise directions, whereas Chebyshev collocation is used for discretization in the wall-normal direction. Time integration of the nonlinear terms for the advective and forcing terms are handled by a third order Runge–Kutta scheme, whereas the viscous terms are handled by a Crank–Nicolson scheme. Details about the code can be found in Lundbladh *et al.* (1999).

For the nonlinear optimization problem, a limited memory quasi-Newton method is used. The algorithm, L-BFGS-B (Byrd *et al.* (1994)), is available on the Internet (the web-link is given in the reference list next to Byrd *et al.* (1994)) and was used without modifications. It is an algorithm well suited for large nonlinear optimization problems, with or without bounds on the control variables.

The BFGS method successively computes secant approximations of the Hessian matrix as the iterations proceed. The algorithm has been shown to work well for many different types of optimization problems. The limited memory BFGS algorithm differs from the standard BFGS algorithm in that it does

not construct a full matrix to approximate the Hessian. Instead only a certain number of gradient and control updates from earlier optimization iterations are stored. These are then used to build an approximation of the Hessian matrix.

Disturbances can be introduced to the flow by applying a forcing in the fringe region, by an external volume forcing, or by adjusting the boundary conditions in order to specify blowing and suction at the wall.

4. Results

Flows with three fundamentally different mechanism for disturbance energy growth are studied: TS waves, optimal disturbances, and stationary cross flow vortices. The TS wave and optimal disturbance are applied to a Blasius boundary layer, and the cross-flow vortices to a Falkner–Skan–Cooke boundary layer. Direct numerical simulations are performed for each one of these perturbations, first without any control, then with linear control, and finally with nonlinear control. The nonlinear optimization loop is initiated with the linear optimal control. Note that the fringe region is excluded from the pictures below.

The energy measure that will be used in the following plots is

$$E(u(x)) = \frac{1}{y_\infty z_l} \int_y \int_z (u_1^2 + v^2 + w^2)\,\mathrm{d}y\,\mathrm{d}z. \tag{29}$$

This energy measure naturally includes the control energy itself.

4.1. *Tollmien-Schlichting waves*

A TS wave is introduced in a Blasius boundary layer and develops as it propagates downstream. The Blasius mean flow is a special case of the Falkner–Skan–Cooke profiles without pressure gradient ($m = 0$) and with no mean flow component in the z-direction.

Two different disturbances are applied, one weak TS wave, and one stronger wave where nonlinear coupling effects start to appear. The weak TS wave is generated by an oscillating two dimensional volume force with the dimensionless frequency $F = 200$, where $F = 2\pi f\nu/U_\infty^2 \times 10^6$. The volume force is centered at $x = 20$ and decays exponentially in both the x- and y-direction.

The stronger wave is generated in the fringe region by forcing toward the least stable Orr–Sommerfeld–Squire eigenmode computed for $\alpha = 0.30$ at $R = 950$, a Reynolds number that corresponds to a spatial location close to the end of the computational box. This TS wave will then be exponentially unstable in the computational box.

Domain and resolution data for the TS wave simulations is given in Table 1, cases 1-6. The Reynolds number at $x = 0$ is $Re = 468.34$ for both the weak and strong disturbance. In the construction of the linear feedback kernels, the base flow profile is taken at $x = 150$. For the nonlinear optimization problem, we specify the observation interval in space and time to $x \in [75, 375]$ and $t \in [0, 750]$, respectively.

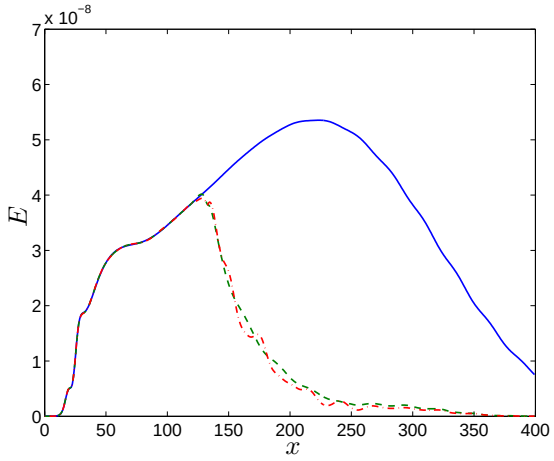

FIGURE 2. The spatial energy growth of a linear TS wave perturbation in a Blasius boundary layer without control from case 1 (solid), with linear control from case 2 (dashed), and nonlinear control from case 3 (dash-dotted). Control is applied in $x \in [75, 225]$. The TS wave is generated as a volume force centered at $x = 20$ for $F = 200$. The linear controller is centered at $x = 150$.

In Figure 2 the streamwise disturbance energy development of weak TS waves are plotted for cases 1-3 in Table 1. A small transient can be seen in the beginning of the energy curve, an effect that is due to the fact that we do not force a clean TS wave. However, as the disturbance evolves downstream, a pure TS wave emerges. The flow is perturbed just upstream of branch I of the neutral stability curve, which is at around $R \approx 507$ ($x \approx 25$), and the disturbance grows exponentially shown, as the solid line in Figure 2. The growth ends when branch II is reached at about $R \approx 723$ ($x \approx 230$). See for example Schmid & Henningson (2001) for details. The dashed line is the disturbance energy development with linear control active. Note that the exponential growth is completely removed and replaced by an exponential decay. With the nonlinear optimal control applied, the energy development follows the dash-dotted line. Since the energy levels are very low and thus nonlinear effects negligible, we can conclude that the deviations originate from differences in the optimization problem and the limitations of the linear control. Analyzing the control signals shows no major differences between the two control approaches. The nonlinear control acts stronger in the beginning of the simulation and also stronger at the upstream part of the spatial control interval. These effects are a direct consequence of the limitations of the linear control problem formulation.

With no control at all, the objective function is $5.291 \cdot 10^{-4}$, and when the linear control is turned on the value is reduced to $5.263 \cdot 10^{-4}$. The relatively low

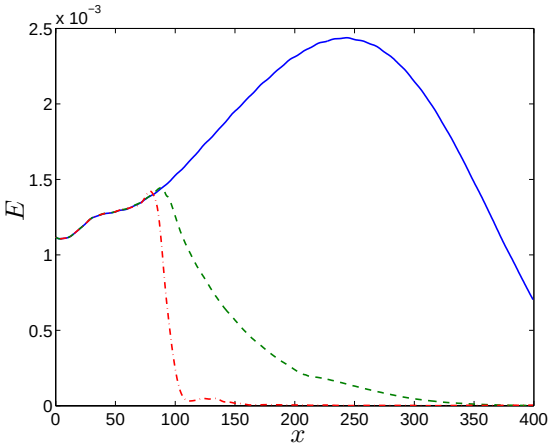

FIGURE 3. The spatial energy growth of a weakly nonlinear TS wave perturbation in a Blasius boundary layer without control from case 4 (solid), with linear control from case 5 (dashed), and nonlinear control from case 6 (dash-dotted). Control is applied in $x \in [75, 225]$. The TS wave is generated at $R = 950$ for $\alpha = 0.30$. The linear controller is centered at $x = 150$.

reduction of the objective function is due to the fact that the simulation time is only as long as is needed for the control signal and the transients it cause to propagate out of the computational box. This means that it is only at the last part of the simulation all transient effects are gone and the disturbance energy is kept on a low level. The nonlinear control reduces the objective function value to $5.260 \cdot 10^{-4}$.

In Figure 3, the disturbance energy development in the streamwise direction for cases 4-6 from Table 1 are plotted. Again, the dashed line denotes the disturbance energy development with linear control turned on. Also for this much stronger TS wave, the exponential growth is completely suppressed. The differences between the nonlinear control and the linear control is more pronounced than for the weak wave. Initially, the nonlinear control signal is higher over the whole control region. The downstream part of the control is quickly dampened to the linear control levels whereas the upstream region stays higher throughout the complete control time. Strong transients with nonlinear interactions are produced by the upstream control. As these transients are convected downstream there is a distinct difference in how the linear and nonlinear control behave. The nonlinear control signal becomes irregular whereas the linear control stays more or less sinusoidal.

The objective function value is reduced from 0.564 to 0.204 by the linear control and further down to 0.077 by the nonlinear control. The nonlinear

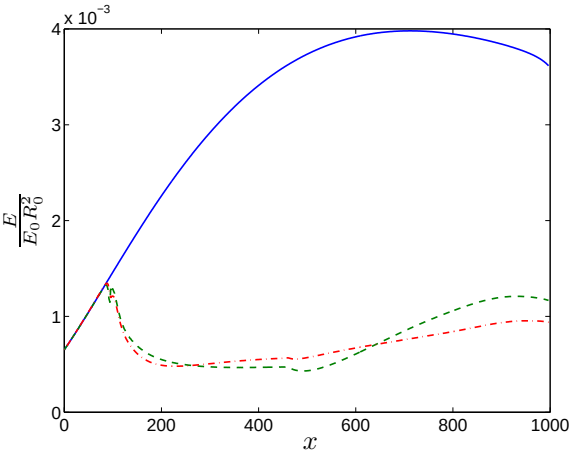

FIGURE 4. Spatial energy growth of a linear optimal disturbance in a Blasius boundary layer without control from case 7 (solid), with linear control from case 8 (dashed), and nonlinear control from case 9 (dash-dotted). Control is applied in $x \in [75, 475]$. The optimal disturbance has the maximum growth at $x = 237.24$. The linear controller is centered at $x = 150$. E_0 is the disturbance energy at $R_0 = 395.4$.

control was picked after 24 iterations in the optimization loop which still has potential to decrease the value more.

4.2. *Optimal disturbances*

Here the performance of the controller for a transiently growing perturbation is studied. The same base flow as for the TS wave simulations is used but now with a larger box in the streamwise direction, see Table 1, cases 7-9, for details.

The spatial optimal perturbations in a Blasius boundary layer have been computed by Andersson *et al.* (1999) and Luchini (2000). The particular optimal spatial perturbation used here is introduced at $R_0 = 395.4$ and then marched forward using the linear equations to the position where $R = 468.34$. By introducing the optimal disturbance in the fringe region, we get a clean perturbation already in the beginning of the computational box. The perturbation is optimized to be the one with maximum growth at $x = 237.24$ in the simulation box.

The linear control kernels are computed from the base flow at position $x = 150$. Furthermore, the spatial and temporal observation region is $x \in [75, 975]$ and $t \in [0, 1500]$ respectively. The solid line in Figure 4 shows the disturbance energy growth without any control. In the same figure, the dashed line marks the evolution of the disturbance energy when linear control is applied, and the dash-dotted line shows the nonlinear control after ten iterations in the

optimization loop. In these controlled cases, we still have transient growth, although substantially weaker. Cathalifaud & Luchini (2000) have computed the optimal control over the whole wall using the linearized boundary layer equations as state equation. Their optimal control is similar in shape as to what we have obtained.

After the disturbance energy reduction in the beginning of the control domain, the nonlinear control casuses the energy to start growing earlier than the linear control does. This is an effect of our choice of spatial observation region. To keep the disturbance from growing to fast behind the control region, stronger control has to be applied, especially at the downstream part of the control region.

No control, for the current observation region, gives an objective function value of $8.955 \cdot 10^{-4}$. Linear control lowers the objective function to $8.695 \cdot 10^{-4}$. After six optimization iterations for the nonlinear control, the objective function reaches $8.531 \cdot 10^{-4}$. The small reduction of the objective function value is due to the fact that the observation time interval captures not only the results at the end of the simulation but also the transient process when the disturbance, already present in the flow, is acted on by the control. The energy curves are just snapshots of the streamwise energy distribution in the flow at the end of the simulation ($T = 1500$).

4.3. *Cross flow vortices*

In a three dimensional boundary layer flow, where the direction of the base flow is a function of the wall normal coordinate, the velocity profile usually has an inflection point. This in turn means that there usually exists an inviscid inflectional instability, see e.g. Gregory *et al.* (1955). This primary instability may result in amplification of oblique travelling waves and of stationary vortices. Local linear stability theory predicts nonstationary modes to be more amplified than stationary modes. In the present work, we have chosen to study a stationary disturbance due to the somewhat smaller computational requirements in such a flow.

If large enough amplitude of the disturbance is used, stationary nonlinearly saturated cross flow vortices will develop downstream. These instabilities have been thoroughly investigated both experimentally, by e.g. Lerche (1997) and Kawakami *et al.* (1999), and numerically, by Högberg & Henningson (1998) and Malik *et al.* (1999). In the present paper only results from lower amplitude disturbance simulations are reported. To mimic a base flow prone to the above behavior, a Falkner–Skan–Cooke boundary layer for an infinitely swept wing with a positive pressure gradient is modeled. Stationary perturbations are introduced in the beginning of the simulation box at $Re = 337.34$ with $m = 0.34207$ and $W_\infty = 1.442$. The same flow case is studied numerically in Högberg & Henningson (1998).

The box size, resolution, and other details are given in Table 1 as cases 10-12. The linear control kernels are constructed from the base flow profile

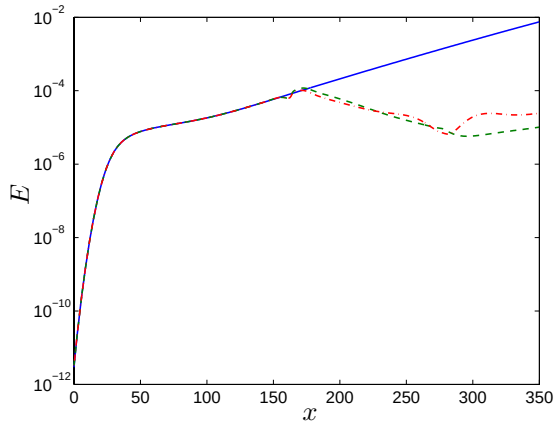

FIGURE 5. Spatial energy growth in the $\beta = 1$ mode of cross flow vortices in a Falkner–Skan–Cooke boundary layer ($m = 0.34207$ and $W_\infty = 1.442$) without control from case 10 (solid), with linear control from case 11 (dashed), and nonlinear control from case 12 (dash-dotted). Control is applied in $x \in [145, 295]$. The linear control kernels are computed with base flow from position $x = 220$.

at $x = 220$. For the nonlinear optimization problem, we have chosen the observation interval in space as $x \in [145, 335]$ and in time as $t \in [0, 800]$.

In Figure 5, the solid line shows the growth of the disturbance energy in the $\beta = 1$ mode. As expected from linear stability theory, it grows exponentially. When applying linear control, the energy growth is efficiently stopped which is shown with the dashed line. However, immediately after we stop controlling the flow, new cross flow vortices begin to form, which is natural due to the presence of an inflectional instability. The nonlinear control, shown as the dash-dotted line in Figure 5, reduces the disturbance growth even further.

When no control is used the objective function is 5.593 and with linear control on it reduces to 0.644. The nonlinear control then decreases it to 0.635 after two iterations.

As for the TS waves and optimal disturbances cases, transient effects linger in the flow until the very last part of the simulation. Therefore, the reduction in objective function is not as large as one might expect from the disturbance energy plot, which again is a snapshot at simulation end time.

5. Summary and conclusions

Direct numerical simulations for three different flow cases have been performed without any control, with an optimal control obtained through a linear feedback loop, and with an optimal control computed from the full nonlinear Navier–Stokes equations in an iterative procedure. The nonlinear optimization problem

Case	Flow	Perturbation	Amp.	Control
1	A	TS wave		none
2	A	TS wave	0.0002	$[75, 225]$
3	A	TS wave	0.0002	$[75, 225]$
4	A	TS wave		none
5	A	TS wave	0.01	$[75, 225]$
6	A	TS wave	0.01	$[75, 225]$
7	B	Optimal		none
8	B	Optimal	0.00001	$[75, 425]$
9	B	Optimal	0.00001	$[75, 425]$
10	C	Cross flow		none
11	C	Cross flow	0.0002	$[145, 295]$
12	C	Cross flow	0.0002	$[145, 295]$

Type	Flow	Resolution	Box
A	Blasius	$576 \times 65 \times 4$	$500 \times 20 \times 12.83$
B	Blasius	$576 \times 65 \times 4$	$1128 \times 20 \times 12.83$
C	FSC	$576 \times 65 \times 24$	$500 \times 10 \times 25.14$

TABLE 1. Summary of different simulations. For all simulations the linear control parameter equals $l = 100$. The nonlinear control parameter equals $\varepsilon = 10^{-5}$. The two different amplitudes for the TS wave simulations correspond to linear and weakly nonlinear disturbances.

is initiated with the linear control in order to speed up the convergence process. Some of the smaller simulations have also been initiated from zero control and they converged to the same control.

The results show that the nonlinear control improves the performance over the linear control markedly in cases where nonlinear effects are significant. Also for perturbations with a linear development there are differences, but a fine tuning of the parameter l in the linear control problem could possibly reduce the difference.

The linear controller results are computed with the same tools as used in Högberg & Henningson (2001) and works well for the studied cases despite its limitations.

The nonlinear control has not been fully converged in any of the simulated cases indicating that one would expect small adjustments to the disturbance energy growth curves. However, the big changes in the control appear in the first few iterations.

For all cases studied the nonlinear control acts more quickly both in space and time. Also the control keeps the disturbance energy levels lower at a downstream location behind the control interval.

Simulations with disturbance amplitudes high enough so that nonlinear effects are more pronounced, will be studied in future work, both for the optimal disturbances and the cross flow vortices.

For nonlinear optimization simulations over larger time intervals and for larger domains, the checkpointing technique mentioned in section 2.1 needs to be applied.

Another important part of the nonlinear optimization problem, is the formulation of the optimization problem itself and the choice of inner products involved. This could have a large impact on the convergence rate of the iterative process and also on how well the "optimal control" will work (see e.g. Protas & Bewley (2002)).

For the linear optimization problem the next natural step is to attempt to reduce the amount of information necessary when computing the control by estimating the state of the flow based on realizable measurement data.

References

Andersson, P., Berggren, M. & Henningson, D. S. 1999 Optimal disturbances and bypass transition in boundary layers. *Phys. Fluids* **11**, 134–150.

Berggren, M. 1995 Optimal control of time evolution systems: Controllability investigations and numerical algorithms. PhD thesis, Rice University, Department of Computational and Applied Mathematics, Houston, Tx 77251-1892.

Berggren, M. 1998 Numerical solution of a flow-control problem: vorticity reduction by dynamic boundary action. *SIAM J. Sci. Comp.* **19** (3), 829–860.

Bewley, T. R. & Liu, S. 1998 Optimal and robust control and estimation of linear paths to transition. *J. Fluid Mech.* **365**, 305–349.

Bewley, T. R., Moin, P. & Temam, R. 2001 DNS-based predictive control of turbulence: an optimal benchmark for feedback algorithms. *J. Fluid Mech.* **447**, 179–225.

Byrd, R. H., Peihuang, L., Nocedal, J. & Zhu, C. 1994 A limited memory algorithm for bound constrained optimization. Technical Report NAM-08. EECS Department, Northwestern University, `http://www.netlib.org/toms/778`.

Cathalifaud, P. & Luchini, P. 2000 Algebraic growth in boundary layers: Optimal control by blowing and suction at the wall. *Eur. J. Mech. B - Fluids* **19**, 469–490.

Glowinski, R. & He, J. 1998 On shape optimization and related issues. In *Computational Methods for Optimal Design and Control* (eds. J. Borggaard, J. Burns, E. Cliff & S. Schreck), pp. 151–179. Birkhäuser, Boston.

Gregory, N., Stuart, J. T. & Walker, W. S. 1955 On the stability of three dimensional boundary layers with application to the flow due to a rotating disk. *Phil. trans. R. Soc. Lond.* **A 248**, 155–199.

Gunzburger, M. D., ed. 1995 *Flow Control*. Springer-Verlag.

Hulsing, K. P. 1999 Methods for computing functional gains for lqr control of partial differential equations. PhD thesis, Virginia Polytechnic Institute and State University.

Högberg, M. & Berggren, M. 2000 Numerical investigation of different discretization approaches for optimal control. *Flow, Turbulence and Combustion* **65** (3/4), 299–320.

Högberg, M. & Bewley, T. R. 2001 Spatially-localized convolution kernels for decentralized control and estimation of transition of plane channel flow. *Automatica* Submitted.

Högberg, M., Chevalier, M., Berggren, M. & Henningson, D. S. 2001 Optimal control of wall bounded flows. Scientific Report FOI-R--0182--SE. Computational Aerodynamics Department, Aeronautics Division, FOI.

Högberg, M. & Henningson, D. S. 1998 Secondary instability of cross-flow vortices in falkner-skan-cooke boundary layers. *J. Fluid Mech.* **368**, 339–357.

Högberg, M. & Henningson, D. S. 2001 Linear optimal control applied to instabilities in spatial boundary layers. *J. Fluid Mech.* Submitted.

Ito, K. & Morris, K. A. 1998 An approximative theory of solutions to operator riccati equations for $\mathcal{H}^\infty$ control. *SIAM J. Control Optim.* **36** (1), 82–99.

Jameson, A. 1989 Computational aerodynamics for aircraft design. *Science* **245**, 361–371.

Joshi, S. S., Speyer, J. L. & Kim, J. 1997 A systems theory approach to the feedback stabilization of infinitesimal and finite-amplitude disturbances in plane poiseuille flow. *J. Fluid Mech.* **332**, 157–184.

Joslin, R. D., Gunzburger, M. D., Nicolaides, R. A., Erlebacher, G. & Hussaini, M. Y. 1997 A Self-contained, Automated Methodology for Optimal Flow Control Validated for Transition Delay. *AIAA Journal* **35** (5), 816–824.

Kawakami, M., Kohama, Y. & Okutsu, M. 1999 Stability characteristic of stationary crossflow vortices in three-dimensional boundary layer. AIAA Paper 99–0811.

Kim, J. & Lim, J. 2000 A linear process in wall-bounded turbulent shear flows. *Phys. Fluids* **12** (8), 1885–1888.

Lerche, T. 1997 Experimentelle Untersuchung nichtlinearen Strukturbildung im Transitionsprozeß einer instabilen Grenzschicht. Fortscrittberichte, VDI, Reihe 7: Strömungstechnik Nr. 310.

Luchini, P. 2000 Reynolds-number-independent instability of the boundary layer over a flat surface: Optimal perturbations. *J. Fluid Mech.* **404**, 289–309.

Lundbladh, A., Berlin, S., Skote, M., Hildings, C., Choi, J., Kim, J. & Henningson, D. S. 1999 An Efficient Spectral Method for Simulations of Incompressible Flow over a Flat Plate. Technical Report TRITA-MEK 1999:11. Royal Institute of Technology, Department of Mechanics, KTH.

Malik, M. R., Li, F., Choudhari, M. M. & Chang, C.-L. 1999 Secondary instability of crossflow vortices and swept-wing boundary layer transition. *J. Fluid Mech.* **399**, 86–115.

Metcalfe, R. W. 1994 Boundary layer control: A brief review. In *Computational Fluid Dynamics '94, Invited Lectures of the Second European CFD Conference* (eds. S. Wagner, J. Periaux & E. Hirschel), pp. 52–60. Stuttgart, Germany: John Wiley & Sons.

Nordström, J., Nordin, N. & Henningson, D. S. 1999 The fringe region technique and the fourier method used in the direct numerical simulation of spatially evolving viscous flows. *SIAM J. Sci. Comp.* **20** (4), 1365–1393.

Protas, B. & Bewley, T. R. 2002 Regularization opportunities in the adjoint analysis of multiscale systems. In *Advances in Turbulence IX* (eds. I. P. Castro, P. E. Hancock & T. G. Thomas). Proceedings of the Ninth European Turbulence Conference.

Reddy, S. C., Schmid, P. J., Baggett, J. S. & Henningson, D. S. 1998 On stability of streamwise streaks and transition thresholds in plane channel flows. *J. Fluid Mech.* **365**, 269–303.

Schmid, P. J. & Henningson, D. S. 2001 *Stability and transition in shear flows*. Springer-Verlag.

Thomas, A. S. W. 1990 Active wave control of boundary-layer transition. In *Viscous Drag Reduction in Boundary Layers* (eds. D. M. Bushnell & J. N. Hefner), *Progress in Astronautics and Aeronautics*, vol. 123. Washington, D.C: American Institute of Aeronautics and Astronautics.

Paper 2

2

Optimal control of wall bounded flows

By Markus Högberg*, Mattias Chevalier*†, Martin Berggren†‡ and Dan S. Henningson*†

Optimal control of transition in channel flow and boundary layer flow is attempted. First the optimization problem is stated and the corresponding adjoint equations used to compute the gradient of the objective function are derived for both the channel flow and boundary layer flow problems. Implementation and numerical issues are discussed, and some details of the implementation are explained. The governing equations used are the incompressible Navier–Stokes equations with appropriate boundary conditions for the two cases. The boundary condition on the wall normal velocity at the walls of the channel, or at the single wall in the boundary layer case, is used as control and is determined in the iterative optimization procedure. The objective function used for the optimization problem contains the perturbation energy and a regularization term on the applied control. The optimization problem is formulated using a continuous formulation in space and time using the primitive variables, velocity and pressure, and is then rewritten in a formulation containing only the wall normal velocity and the wall normal vorticity. An existing solver for the incompressible Navier–Stokes equations using this formulation can then also be used to solve the associated adjoint problem. Implementation is straightforward using this formulation and the efficiency of the original solver is maintained. To test the performance of the solver of the optimization problem, the derived formulation is applied on different stages of the oblique transition scenario in the channel flow case. In a parallel Falkner–Skan–Cooke flow successful control of an inviscid instability is reported, and in the spatial Blasius flow the energy growth of a Tollmien–Schlichting wave is efficiently inhibited.

1. Introduction

In the last decade, one topic in fluid mechanics that has been subject to an increasing interest is *flow control*. The explosive development in computer technology has made it possible to approach these problems from a numerical point of view, and also to construct small devices to be used for measurements and actuation in experiments. The numerical approach to flow control can for

*Department of Mechanics, Royal Institute of Technology (KTH), SE-100 44 Stockholm, Sweden
†The Swedish Defence Research Agency (FOI), SE-172 90 Stockholm, Sweden
‡Department of Scientific Computing, Uppsala University

example be used to design the shape of a wing to minimize drag or to solve some other optimization problem. Mathematical aspects of the flow control problem is the topic of the books edited by Gunzburger (1995) and Sritharan (1998). Computational approaches to flow control are reviewed in the paper by Hinze & Kunish (2000). Optimal control of channel flow using direct numerical simulations was previously considered using by Bewley *et al.* (2001) and using large eddy simulations by Collis *et al.* (2000). In addition to channel flow Joslin *et al.* (1997) also considered the boundary layer case with a two dimensional flow in direct numerical simulations.

In this work we consider the problem of control of transition from laminar to turbulent flow in a channel and a boundary layer. In many applications there is a large potential benefit from the ability to prevent transition whereas in other applications the turbulent state is the desired one. Our objective is to delay or prevent transition at low Reynolds numbers, particularly focusing on the bypass transition (Morkovin (1969)) scenarios, not originating from an exponential instability. The problem of bypass transition is important in many practical applications, and considerable amounts of research has been done on this subject see e.g. the recent book by Schmid & Henningson (2001).

2. Optimization problem formulations

The formulation of an optimal control problem is based on three important decisions. The choice of governing equations, determining what means of actuation to use, and what properties of the flow to control. For a particular flow geometry and with given fluid properties, these choices have to be made with care.

In this work the governing equations are the incompressible Navier–Stokes equations. In a recent study, successful application of feedback controllers computed from the linearized Navier–Stokes equations was performed by Högberg & Bewley (2001) in temporal channel flow. Changes in the mean flow is not easily taken into account using this formulation. Thus, a proper treatment of problems where this is important, such as a flow with local separation, requires the use of the full Navier–Stokes equations.

Since no particular quantity is known that establishes where we are on the path to transition the choice of objective function is difficult. The mean skin friction drag could be used as an indicator, since it has a jump at transition, and can be used to define a transition point, as for example in Reddy *et al.* (1998). On the other hand, Bewley *et al.* (2001) showed that the mean drag was not a good choice for the objective function when the purpose was to relaminarize turbulence in a channel flow, and concluded that the turbulent kinetic energy was a more appropriate choice. Since we are interested in control of transition rather than turbulence, the energy of the deviation from the mean flow appears to be an appropriate quantity to minimize. An increased physical understanding of the transition process and the crucial mechanisms

of turbulence could provide a guide to the best choice of objective function as pointed out by Kim & Lim (2000).

It is important to choose the properties of the control in such a way that it is able to do its task in an efficient way. For our study, we have chosen to use blowing and suction at the wall during a specified period in time. The state of the flow is observed during another, possibly overlapping, period in time. When a spatially rather than a temporally evolving flow is considered it is physically meaningful to specify also the spatial extent of the control and observation regions. The control is restricted to have zero mass flux, in order to limit the ability to affect the mean flow and focus the control effort on the perturbations.

The gradient of the objective function may be expressed in terms of the solution of an *adjoint equation*. Here, we discretize the expressions for the adjoint equations and the gradient that have been derived on the "continuous" level. An alternative is to discretize the Navier–Stokes equations and the objective function and *derive* the adjoint equations and the gradient expression on the discrete level. The latter approach leads to more accurate gradient directions, but it seems difficult to apply for the present discretizations. Issues related to the errors introduced by the approximative (continuous) formulation are discussed in e.g. Glowinski & He (1998) and Gunzburger (1998). The use of the continuous formulation is motivated by the findings in Högberg & Berggren (2000) where one conclusion was that it is sufficient to use the approximative (continuous) formulation in order to control strong instabilities. It was noted that in such cases most of the reduction of the objective function is achieved in the first few iterations, and additional iterations only result in a fine tuning of the control. The drawback is that it will require more iterations to reach the true optimal solution, if it is even possible, than with the discrete formulation.

2.1. *Governing equations*

In this section we consider the channel flow problem and the details of the method used to solve the optimization problem. The boundary layer problem is basically an extension of the channel flow case. The differences are outlined in section 2.3, and a full description is provided in Appendix A.

Our computational domain depicted in Figure 1 is

$$\Omega = (-x_L/2, x_L/2) \times (-1, 1) \times (-z_L/2, z_L/2),$$

in x, y, z, and we define

$$\Gamma_L = \Omega(y = -1), \quad \Gamma_U = \Omega(y = 1) \quad \text{and} \quad Q = \Omega \times (0, T).$$

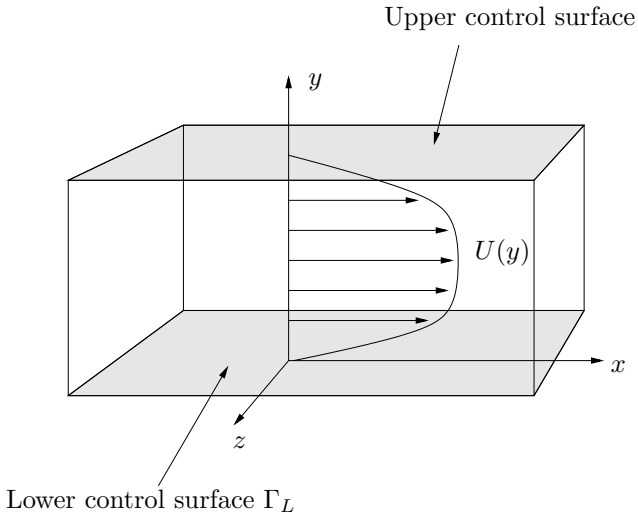

FIGURE 1. Geometry of flow domain Ω for channel flow simulations.

The non-dimensional, incompressible Navier–Stokes equations with a Reynolds number, Re, based on the centerline velocity and half the channel height are,

$$\begin{cases} \dfrac{\partial u}{\partial t} + (u \cdot \nabla)u - \dfrac{1}{Re}\Delta u + \nabla \pi = -\nabla P & \text{in } Q, \\ \nabla \cdot u = 0 & \text{in } Q, \\ u|_{t=0} = u_0, \end{cases} \tag{1}$$

where $u = (u_1, v, w)$ is the velocity vector, π is the pressure and ∇P represents the pressure gradient driving the flow and can either be constant or used to ensure constant mass flux. Periodic boundary conditions in x and z, and control through blowing and suction together with a no-slip condition for the directions parallel to the wall gives the complete set of boundary conditions,

$$\begin{gathered} u|_{x=-x_L/2} = u|_{x=x_L/2}, \\ u|_{z=-z_L/2} = u|_{z=z_L/2}, \\ e_i \cdot u|_{y=-1} = \begin{cases} \varphi_L^T \psi_L = \sum_{m=1}^{M_L} \varphi_{L,m}(t)\, \psi_{L,m}(x,z) & \text{in } (T_1^c, T_2^c) \quad \text{for } i = 2, \\ 0 & \text{otherwise}, \end{cases} \\ e_i \cdot u|_{y=1} = \begin{cases} \varphi_U^T \psi_U = \sum_{m=1}^{M_U} \varphi_{U,m}(t)\, \psi_{U,m}(x,z) & \text{in } (T_1^c, T_2^c) \quad \text{for } i = 2, \\ 0 & \text{otherwise}, \end{cases} \end{gathered} \tag{2}$$

where e_i are unit basis vectors in the coordinate directions, and ψ are basis functions for the control designed to have zero net mass flux. We can now

introduce the control variable φ defined as:

$$\varphi = (\varphi_L, \varphi_U)^T, \begin{cases} \varphi_L = (\varphi_{L,1}, \dots, \varphi_{L,M_L})^T, \\ \varphi_U = (\varphi_{U,1}, \dots, \varphi_{U,M_U})^T. \end{cases}$$

To completely specify the optimal control problem we also need an objective function. If we choose to minimize the energy of the deviation from a target velocity distribution, the objective function is:

$$J(\varphi) = \frac{\varepsilon}{2} \int_{T_1^c}^{T_2^c} \int_{\Gamma} |v|^2 \, \mathrm{d}\Gamma \, \mathrm{d}t + \frac{1}{2} \int_{T_1^o}^{T_2^o} \int_{\Omega} |u - u_T|^2 \, \mathrm{d}Q, \tag{3}$$

where (T_1^c, T_2^c) is the control time period and (T_1^o, T_2^o) is the observation time period. The target velocity profile is denoted u_T. The optimization problem is then: find φ^* which satisfies

$$J(\varphi^*) \leq J(\varphi) \quad \forall \; v(\varphi)|_\Gamma \in \mathcal{U}_{\mathrm{ad}}$$

where $\mathcal{U}_{ad}$ has been used to denote the set of *admissible controls* which is a subset of $L^2((T_1^c, T_2^c); \mathbb{R}^{M_L+M_U})$.

2.2. *Derivation of objective function gradient*

The gradient of the objective function ∇J is defined by

$$\begin{aligned} \delta J(\varphi) &= \lim_{s \to 0} \frac{J(\varphi + s\,\delta\varphi) - J(\varphi)}{s} = \langle \nabla J, \delta\varphi \rangle \\ &= \left\langle \frac{\partial J}{\partial \varphi_L}, \delta\varphi \right\rangle + \left\langle \frac{\partial J}{\partial \varphi_U}, \delta\varphi \right\rangle, \end{aligned} \tag{4}$$

where $\delta\varphi$ is the first variation of the control. The functional δJ is the first variation of J with respect to $\delta\varphi$. To find an expression for ∇J we start by differentiating the objective function (3) to get,

$$\delta J(\varphi) = \varepsilon \int_{T_1^c}^{T_2^c} \int_{\Gamma} \delta v \, v \, \mathrm{d}\Gamma \, \mathrm{d}t + \int_{T_1^o}^{T_2^o} \int_{\Omega} \delta u \cdot (u - u_T) \, \mathrm{d}Q, \tag{5}$$

where $\delta v = e_2 \cdot \delta u$ and δu is the first variation of u with respect to $\delta\varphi$. To find an expression for the relation between δu and $\delta\varphi$ we differentiate state equation (1),

$$\begin{cases} \dfrac{\partial \delta u}{\partial t} + (\delta u \cdot \nabla) u + (u \cdot \nabla) \delta u - \dfrac{1}{Re} \Delta \delta u + \nabla \delta\pi = 0 & \text{in } Q, \\ \nabla \cdot \delta u = 0 & \text{in } Q, \\ \delta u|_{t=0} = 0, \end{cases} \tag{6}$$

and boundary conditions (2),

$$\begin{aligned}
\delta u|_{x=-x_L/2} &= \delta u|_{x=x_L/2}, \\
\delta u|_{z=-z_L/2} &= \delta u|_{z=z_L/2}, \\
e_i \cdot \delta u|_{y=-1} &= \begin{cases} \delta\varphi_L^T \psi_L = \sum_{m=1}^{M_L} \delta\varphi_{L,m}(t)\psi_{L,m}(x,z) & \text{in } (T_1^c, T_2^c) \quad \text{for } i=2, \\ 0 & \text{otherwise,} \end{cases} \\
e_i \cdot \delta u|_{y=1} &= \begin{cases} \delta\varphi_U^T \psi_U = \sum_{m=1}^{M_U} \delta\varphi_{U,m}(t)\psi_{U,m}(x,z) & \text{in } (T_1^c, T_2^c) \quad \text{for } i=2, \\ 0 & \text{otherwise.} \end{cases}
\end{aligned} \tag{7}$$

Now we introduce a vector function $p = p(x, y, z, t)$ such that $e_i \cdot p = p_i$ and require p to satisfy the boundary conditions:

$$\begin{aligned}
p|_{x=-x_L/2} &= p|_{x=x_L/2}, \\
p|_{z=-z_L/2} &= p|_{z=z_L/2}, \\
p|_{y=-1} &= p|_{y=1} = 0.
\end{aligned} \tag{8}$$

The boundary conditions may be chosen during the derivation but in order to simplify the presentation they are introduced already at this point. Taking the dot product between p and equation (6) and integrating over Q yields

$$\int_Q p \cdot \Big(\underbrace{\frac{\partial \delta u}{\partial t}}_{1} + \underbrace{(\delta u \cdot \nabla) u}_{2} + \underbrace{(u \cdot \nabla)\delta u}_{3} - \underbrace{\frac{1}{Re}\Delta \delta u}_{4} + \underbrace{\nabla \delta\pi}_{5} \Big) \, \mathrm{d}Q = 0. \tag{9}$$

Then, step by step, we apply integration by parts to move derivatives from δu to p. We start with the first term in the integral (9), containing the time derivative:

$$\begin{aligned}
\int_Q p \cdot \frac{\partial \delta u}{\partial t} \, \mathrm{d}Q &= \int_\Omega \left(p(T) \cdot \delta u(T) - p(0) \cdot \delta u(0) \right) \mathrm{d}\Omega - \int_Q \delta u \cdot \frac{\partial p}{\partial t} \, \mathrm{d}Q \\
&= \int_\Omega p(T) \cdot \delta u(T) \, \mathrm{d}\Omega - \int_Q \delta u \cdot \frac{\partial p}{\partial t} \, \mathrm{d}Q,
\end{aligned} \tag{10}$$

where we have used that $\delta u(t=0)=0$. Then consider the fourth and fifth terms in integral (9), involving $\Delta\delta u$ and $\delta\pi$:

$$
\begin{aligned}
&-\frac{1}{Re}\int_Q p\cdot\Delta\delta u\,\mathrm{d}Q+\int_Q(p\cdot\nabla)\delta\pi\,\mathrm{d}Q\\
&\quad=-\frac{1}{Re}\int_0^T\Big[\int_\Gamma\frac{\partial\delta u}{\partial n}\cdot p\,\mathrm{d}\Gamma-\int_\Omega\nabla p:\nabla\delta u\,\mathrm{d}\Omega\Big]\mathrm{d}t\\
&\qquad+\int_0^T\Big[\int_\Gamma n\cdot p\,\delta\pi\,\mathrm{d}\Gamma-\int_\Omega\delta\pi(\nabla\cdot p)\,\mathrm{d}\Omega\Big]\mathrm{d}t\\
&\quad=\int_0^T\!\!\int_\Gamma p\cdot\left(n\,\delta\pi-\frac{1}{Re}\frac{\partial\delta u}{\partial n}\right)\mathrm{d}\Gamma\mathrm{d}t\\
&\qquad+\frac{1}{Re}\int_0^T\Big[\int_\Gamma\delta u\cdot\frac{\partial p}{\partial n}\mathrm{d}\Gamma-\int_\Omega\delta u\cdot\Delta p\,\mathrm{d}\Omega\Big]\mathrm{d}t-\int_Q\delta\pi(\nabla\cdot p)\,\mathrm{d}Q\\
&\quad=\frac{1}{Re}\int_{T_1^c}^{T_2^c}\Big[\delta\varphi_L^T\int_{\Gamma_L}\psi_L\frac{\partial p_2}{\partial n}\,\mathrm{d}\Gamma+\delta\varphi_U^T\int_{\Gamma_U}\psi_U\frac{\partial p_2}{\partial n}\,\mathrm{d}\Gamma\Big]\mathrm{d}t\\
&\qquad-\frac{1}{Re}\int_Q\delta u\cdot\Delta p\,\mathrm{d}Q-\int_Q\delta\pi(\nabla\cdot p)\,\mathrm{d}Q.
\end{aligned}
\tag{11}
$$

where : denotes a complete contraction; that is,

$$
\nabla p:\nabla\delta u=\sum_{i,j=1}^{3}\frac{\partial(e_i\cdot p)}{\partial x_j}\frac{\partial(e_i\cdot\,\delta u)}{\partial x_j}.
\tag{12}
$$

In the third equality of (11), we use the boundary condition on δu from (7) and on p from (8).

We can simply rewrite the second term in (9):

$$
\int_Q p\cdot(\delta u\cdot\nabla)u\,\mathrm{d}Q=\int_Q\delta u\cdot(\nabla u)^T p\,\mathrm{d}Q.
\tag{13}
$$

For the third term in (9), we use Gauss theorem, the boundary condition on p in (8) and the incompressibility condition,

$$\begin{aligned}
&\int_Q p \cdot (u \cdot \nabla)\delta u \,\mathrm{d}Q \\
&\quad = \int_0^T\!\!\int_\Gamma (p \cdot \delta u)(n \cdot u) \,\mathrm{d}\Gamma \,\mathrm{d}t \\
&\qquad - \int_Q (p \cdot \delta u)(\nabla \cdot u) \,\mathrm{d}Q - \int_Q \delta u \cdot (u \cdot \nabla)p \,\mathrm{d}Q \\
&\quad = -\int_Q \delta u \cdot (u \cdot \nabla)p \,\mathrm{d}Q,
\end{aligned} \tag{14}$$

Then by inserting (10), (11), (13) and (14) into (9) we get:

$$\begin{aligned}
&\int_\Omega p(T)\,\delta u(T) \,\mathrm{d}\Omega \\
&+ \frac{1}{Re}\int_{T_1^c}^{T_2^c}\left[\delta\varphi_L^T \int_{\Gamma_L} \psi_L \frac{\partial p_2}{\partial n} \,\mathrm{d}\Gamma + \delta\varphi_U^T \int_{\Gamma_U} \psi_U \frac{\partial p_2}{\partial n} \,\mathrm{d}\Gamma\right]\mathrm{d}t \\
&+ \int_Q \delta u \cdot \left(-\frac{\partial p}{\partial t} - \frac{1}{Re}\Delta p + (\nabla u)^T p - (u \cdot \nabla)p\right)\mathrm{d}Q \\
&- \int_Q \delta\pi\,(\nabla \cdot p)\,\mathrm{d}Q = 0.
\end{aligned} \tag{15}$$

If we then require p to satisfy the adjoint equations:

$$\begin{cases}
-\dfrac{\partial p}{\partial t} - \dfrac{1}{Re}\Delta p + (\nabla u)^T p - (u \cdot \nabla)p + \nabla\sigma = \begin{cases} u - u_T & \text{in } (T_1^o, T_2^o) \\ 0 & \text{otherwise} \end{cases} & \text{in } Q, \\
\nabla \cdot p = 0 & \text{in } Q, \\
p|_{t=T} = 0, &
\end{cases} \tag{16}$$

with the boundary conditions from (8) and where σ is a scalar field (the "adjoint pressure"). Then (15) becomes

$$\int_{T_1^o}^{T_2^o}\!\!\int_\Omega \delta u \cdot (u - u_T) \,\mathrm{d}Q - \int_Q \delta u \cdot \nabla\sigma \,\mathrm{d}Q = 0, \tag{17}$$

since $\partial p_2/\partial n$ is zero at the boundaries $y = \pm 1$. This follows from the fact that the no-slip condition implies

$$\frac{\partial p_1}{\partial x} = \frac{\partial p_3}{\partial z} = 0$$

on the walls and from the condition requiring p to be divergence-free. Also, note that the initial condition for the adjoint equations (16) is set at $t = T$ and that the equations are integrated backwards in time.

Integrating the second term in the integral (17) by parts yields

$$\begin{aligned} -\int_Q \delta u \cdot \nabla \sigma \,\mathrm{d}Q &= -\int_0^T\!\!\int_\Gamma n \cdot \delta u \, \sigma \,\mathrm{d}\Gamma \,\mathrm{d}t + \int_Q \sigma \nabla \cdot \delta u \,\mathrm{d}Q \\ &= -\int_0^T\!\!\int_\Gamma n \cdot \delta u \, \sigma \,\mathrm{d}\Gamma \,\mathrm{d}t, \end{aligned} \tag{18}$$

since $\nabla \cdot \delta u = 0$. Inserting the boundary condition on δu from (7) into (18) we get,

$$\begin{aligned} &-\int_0^T\!\!\int_\Gamma n \cdot \delta u \, \sigma \,\mathrm{d}\Gamma \,\mathrm{d}t \\ &\quad = \int_{T_1^c}^{T_2^c}\!\!\int_{\Gamma_L} \delta\varphi_L^T \psi_L \sigma \,\mathrm{d}\Gamma \,\mathrm{d}t - \int_{T_1^c}^{T_2^c}\!\!\int_{\Gamma_U} \delta\varphi_U^T \psi_U \sigma \,\mathrm{d}\Gamma \,\mathrm{d}t. \end{aligned} \tag{19}$$

If we now insert (18) and (19) into (17) we get,

$$\begin{aligned} &\int_{T_1^c}^{T_2^c} \left[\delta\varphi_L^T \int_{\Gamma_L} \psi_L \sigma \,\mathrm{d}\Gamma - \delta\varphi_U^T \int_{\Gamma_U} \psi_U \sigma \,\mathrm{d}\Gamma \right] \mathrm{d}t \\ &\quad + \int_{T_1^o}^{T_2^o}\!\!\int_\Omega \delta u \cdot (u - u_T) \,\mathrm{d}Q = 0. \end{aligned} \tag{20}$$

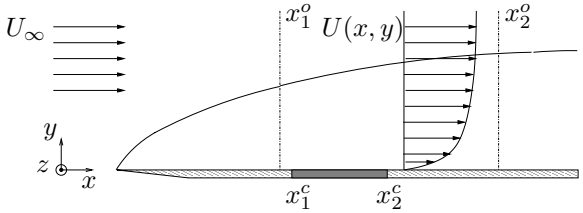

FIGURE 2. Geometry for boundary layer flow simulations.

Finally we can now insert (20) into (5) using (2) to eliminate δu

$$\begin{aligned}\delta J(\varphi) &= \left\langle \frac{\partial J}{\partial \varphi_L}, \delta\varphi \right\rangle + \left\langle \frac{\partial J}{\partial \varphi_U}, \delta\varphi \right\rangle \\ &= \int_{T_1^c}^{T_2^c} \Big\{ \delta\varphi_L^T \Big[\int_{\Gamma_L} \psi_L \left(\varepsilon \varphi_L^T \psi_L - \sigma \right) \mathrm{d}\Gamma \Big] \\ &\qquad + \delta\varphi_U^T \Big[\int_{\Gamma_U} \psi_U \left(\varepsilon \varphi_U^T \psi_U + \sigma \right) \mathrm{d}\Gamma \Big] \Big\} \mathrm{d}t.\end{aligned} \tag{21}$$

¿From expression (21) we can identify the gradient of the objective function (3),

$$\frac{\partial J}{\partial \varphi_L} = \int_{\Gamma_L} \psi_L \left(\varepsilon \varphi_L^T \psi_L - \sigma \right) \mathrm{d}\Gamma, \tag{22}$$

and

$$\frac{\partial J}{\partial \varphi_U} = \int_{\Gamma_U} \psi_U \left(\varepsilon \varphi_U^T \psi_U + \sigma \right) \mathrm{d}\Gamma. \tag{23}$$

2.3. *Extension to boundary layer*

Only minor changes are needed to rephrase the channel flow problem to the boundary layer flow depicted in Figure 2. A complete derivation of the boundary layer counterpart of the channel flow optimization problem can be found in Appendix A. In this section only the key differences will be pointed out and commented.

The growing boundary layer is modeled by

$$\begin{cases} \dfrac{\partial u}{\partial t} + (u \cdot \nabla)u - \dfrac{1}{Re}\Delta u + \nabla \pi = \lambda(x)(U - u) & \text{in } Q, \\ \nabla \cdot u = 0 & \text{in } Q, \\ u|_{t=0} = u_0, \end{cases} \tag{24}$$

with periodic boundary conditions in the horizontal directions, that is, the x- and z-directions,

$$\begin{aligned} u|_{x=-x_l/2} &= u|_{x=x_l/2}, \\ u|_{z=-z_l/2} &= u|_{z=z_l/2}. \end{aligned} \tag{25}$$

The term $\lambda(x)(U-u)$ is a forcing term used to make the flow situation sketched in Figure 2 periodic, enabling the use of Fourier discretization in simulations of the physical flow. This is known as a fringe region technique and is described further in Lundbladh *et al.* (1999) and analyzed by Nordström *et al.* (1999). Left to be specified are the conditions on the wall and in the free-stream. On the wall the boundary condition for the horizontal velocities is a no-slip condition and the wall normal velocity v_c is given by the control. The free-stream boundary condition should be applied at $y = y_{\text{fst}}$ where the flow is not influenced by the existence of the boundary layer, but the simulation box has to be of reasonable height. An artificial boundary condition modeling the existence of the free-stream is thus used to allow truncation of this large domain. Here a Neumann condition is used at the artificial free-stream boundary. This choice requires that the simulation box is high enough for the perturbations in the boundary layer not to influence the flow at the upper boundary.

$$\begin{aligned} u|_{y=y_{\text{fst}}} &= U_\infty \quad \left(\text{which is approximated by} \quad \left.\frac{\partial u}{\partial n}\right|_{\Gamma_u} = 0\right), \\ u|_{\Gamma_c} &= n v_c, \\ u|_{\Gamma_l \setminus \Gamma_c} &= 0, \end{aligned} \tag{26}$$

where Γ_u and Γ_l represent the upper and lower part of the boundary respectively. The part of the boundary where control is applied is denoted Γ_c.

As for the channel flow case we expand the control v_c in basis functions $\psi_{l,m}$ with zero mass flux, where $\varphi_{l,m}$ are time dependent coefficients for the basis functions,

$$v_c(x,z,t) = \begin{cases} \varphi_l^T \psi_l = \displaystyle\sum_{m=1}^{M} \varphi_{l,m}(t)\psi_{l,m}(x,z) & \text{in } (T_1^c, T_2^c), \\ 0 & \text{otherwise.} \end{cases} \tag{27}$$

Where we have introduced the control vector φ_l defined as:

$$\varphi_l = (\varphi_{l,1}, \ldots, \varphi_{l,M}).$$

Comparing with the corresponding equation for channel flow, equation (1) and the associated boundary conditions, there are two differences. The boundary condition at the upper wall is now replaced by a free-stream velocity condition. Also the aforementioned fringe forcing term which is needed only for spatial simulations is added to the right hand side. The scalar function $\lambda = \lambda(x)$ is

nonzero only in the fringe region and is defined as follows:

$$\lambda(x) = \lambda_{\max}\left[S\left(\frac{x - x_{\text{start}}}{\Delta_{\text{rise}}}\right) - S\left(\frac{x - x_{\text{end}}}{\Delta_{\text{fall}}} + 1\right)\right]$$

where $\lambda_{\max}$, x_{start}, x_{end}, Δ_{rise} and Δ_{fall} are parameters used to specify the strength, extent and shape of the fringe forcing. The S-function is defined as

$$S(r) = \begin{cases} 0 & r \leq 0, \\ \dfrac{1}{1 + \exp(1/(1-r) + 1/r)} & 0 < r < 1, \\ 1 & r \geq 1. \end{cases}$$

Another difference from the channel flow problem formulation appears in the second term of the objective function J, equation (3), where the observation of state can now be limited in space as well as in time which yields,

$$J(\varphi_l) = \frac{\varepsilon}{2}\int_{T_1^c}^{T_2^c}\int_{\Gamma_c} |v_c|^2 \,\mathrm{d}\Gamma\,\mathrm{d}t + \frac{1}{2}\int_{T_1^o}^{T_2^o}\int_{\Omega_o} |u - u_T|^2 \,\mathrm{d}Q, \tag{28}$$

where (T_1^c, T_2^c) is the control time period and (T_1^o, T_2^o) is the observation time period and Ω_o is the part of the spatial domain Ω where the state of the flow is observed. This is only used for spatial simulations.

As for the channel flow derivation, we get to the stage where the adjoint equations with the variables p and σ are introduced:

$$\begin{cases} -\dfrac{\partial p}{\partial t} + (\nabla u)^T p - (u \cdot \nabla)p & \\ \quad -\dfrac{1}{Re}\Delta p + \lambda(x)p + \nabla\sigma = \begin{cases} u - u_T & \text{in } (T_1^o, T_2^o) \times \Omega_o \\ 0 & \text{otherwise} \end{cases} & \text{in } Q, \\ \nabla \cdot p = 0 & \text{in } Q, \\ p|_{t=T} = 0. & \end{cases} \tag{29}$$

along with the boundary conditions:

$$\begin{aligned} p|_{x=-x_l/2} &= p|_{x=x_l/2}, \\ p|_{z=-z_l/2} &= p|_{z=z_l/2}, \\ p|_{\Gamma_l} &= 0, \\ p|_{y=y_{\text{fst}}} &= 0, \quad \left(\text{which is approximated by} \quad \left.\frac{\partial p}{\partial n}\right|_{\Gamma_u} = 0\right). \end{aligned} \tag{30}$$

As with the free-stream boundary condition in (26) we have introduced an artificial boundary, to truncate the adjoint domain, where the adjoint "free-stream" is modeled.

Due to the fringe forcing, the additional term $\lambda(x)p$ has to be included in the adjoint equations. The forcing $u - u_T$ is now confined to the spatial domain

Ω_o due to the variable spatial extent of the observation. These adjustments lead to following the expression for the gradient:

$$\frac{\partial J}{\partial \varphi_l} = \int_{\Gamma_c} \psi_l \left(\varepsilon \varphi_l^T \psi_l - \sigma \right) \mathrm{d}\Gamma. \tag{31}$$

3. Adapting to the simulation codes

3.1. *Reformulation of the adjoint equations*

To be able to use existing spectral channel flow and boundary layer flow codes by Lundbladh *et al.* (1992) and Lundbladh *et al.* (1999) respectively, we need to reformulate the adjoint equations into a similar form to the one used there. The simulation code for the boundary layer problem is based on the channel flow code and the solution procedure is identical. The Navier–Stokes equations are implemented in a $v - \omega$ formulation, where linear and nonlinear terms are treated separately. We can write the adjoint equations (16) or (29) as,

$$\begin{cases} -\dfrac{\partial p}{\partial t} - \dfrac{1}{Re}\Delta p - H + \nabla(u \cdot p) + \nabla\sigma = 0, \\ \nabla \cdot p = 0, \\ p|_{t=T} = 0, \end{cases} \tag{32}$$

with the boundary conditions (8) or (30), and where H in the following denotes either H_{ch} or H_{bl} corresponding to the forcing terms in the channel and boundary layer cases respectively. In order to avoid derivatives of u in the adjoint equations, terms involving such derivatives are reformulated. Using the identity

$$u \times (\nabla \times p) - 2(\nabla p)^T u + \nabla(u \cdot p) = (\nabla u)^T p - (u \cdot \nabla) p$$

the forcing in the channel flow case is given by

$$H_{ch} = -u \times (\nabla \times p) + 2(\nabla p)^T u + \begin{cases} u - u_T & \text{in } (T_1^o, T_2^o), \\ 0 & \text{otherwise,} \end{cases}$$

and in the boundary layer case we use

$$H_{bl} = -u \times (\nabla \times p) + 2(\nabla p)^T u - \lambda(x) p + \begin{cases} u - u_T & \text{in } (T_1^o, T_2^o) \times \Omega_o, \\ 0 & \text{otherwise,} \end{cases}$$

but apart from this, the procedure is the same in both cases. If we take the divergence of equation (32) we get a Poisson equation for the adjoint pressure:

$$\Delta\sigma = \nabla \cdot H - \Delta(u \cdot p). \tag{33}$$

We can then apply the Laplace operator to equation (32), take the second component, and combine with (33) to get:

$$-\frac{\partial \Delta p_2}{\partial t} - \frac{1}{Re}\Delta^2 p_2 - \left(\frac{\partial^2}{\partial x^2} + \frac{\partial^2}{\partial z^2} \right) H_2 + \frac{\partial}{\partial y}\left(\frac{\partial H_1}{\partial x} + \frac{\partial H_3}{\partial z} \right) = 0. \tag{34}$$

Then we take the second component of the equation obtained by taking the curl of equation (32) and again making use of (33) to get,

$$-\frac{\partial(\nabla \times p)_2}{\partial t} - \frac{1}{Re}\Delta(\nabla \times p)_2 - \left(\frac{\partial H_1}{\partial z} - \frac{\partial H_3}{\partial x}\right) = 0. \tag{35}$$

We can write equation (34) as a system of two second order equations:

$$\begin{cases} -\dfrac{\partial \phi}{\partial t} = h_{p_2} + \dfrac{1}{Re}\Delta\phi, \\ \Delta p_2 = \phi, \\ p_2(y = \pm 1) = \dfrac{\partial p_2}{\partial y}(y = \pm 1) = 0, \end{cases} \tag{36}$$

where

$$h_{p_2} = \left(\frac{\partial^2}{\partial x^2} + \frac{\partial^2}{\partial z^2}\right) H_2 - \frac{\partial}{\partial y}\left(\frac{\partial H_1}{\partial x} + \frac{\partial H_3}{\partial z}\right). \tag{37}$$

Written on the same form equation (35) reads:

$$\begin{cases} -\dfrac{\partial(\nabla \times p)_2}{\partial t} = h_{(\nabla \times p)_2} + \dfrac{1}{Re}\Delta(\nabla \times p)_2, \\ (\nabla \times p)_2(y = \pm 1) = 0, \end{cases} \tag{38}$$

where

$$h_{(\nabla \times p)_2} = \left(\frac{\partial H_1}{\partial z} - \frac{\partial H_3}{\partial x}\right). \tag{39}$$

Equations (36), (37), (38) and (39) are identical to those solved by the spectral channel flow and boundary layer codes with slight changes to H and a negative time derivative. Since the adjoint equations are solved backwards in time, we can in practice use the same solver.

3.2. *Gradient evaluation*

In the gradient of the objective function we need the adjoint pressure at the wall. This is not available directly since we have eliminated the adjoint pressure term from the equations, and thus the pressure is not computed explicitly. If we evaluate equation (16) or (29) at the walls, we get

$$\begin{aligned} \sigma_x\Big|_W &= \frac{1}{Re}\frac{\partial^2 p_1}{\partial y^2}\Big|_W + v\frac{\partial p_1}{\partial y}\Big|_W, \\ \sigma_z\Big|_W &= \frac{1}{Re}\frac{\partial^2 p_3}{\partial y^2}\Big|_W + v\frac{\partial p_3}{\partial y}\Big|_W, \end{aligned} \tag{40}$$

where W denotes the value at the wall and v is the wall normal velocity at the wall, or rather the control input. Note that in the channel flow case there are two walls and in the boundary layer flow there is only one. Since the constant part of the adjoint pressure disappears in the integral over the basis functions ψ in (22) and (23) we can compute the objective function gradient by integration of these adjoint pressure gradients at the wall.

4. Implementation issues

4.1. *Simulation codes*

The implementation of the adjoint solver is based on existing direct numerical simulation codes for channel and boundary layer flow. These codes have been extensively used and are thoroughly verified. The channel flow code is described in Lundbladh *et al.* (1992) and the boundary layer code in Lundbladh *et al.* (1999). The time marching is performed with a Runge–Kutta method for advective terms and a Crank–Nicolson scheme for the viscous terms. A spectral method described in Canuto *et al.* (1988) is used with a Fourier discretization in x and z, and a Chebyshev method in y. The discretization of, and the solution procedure for, the Navier–Stokes equations is described in Lundbladh *et al.* (1992). The adjoint equation is solved in exactly the same way, with the formulation of the equations described in section 3.1. For the boundary layer case the code described in Lundbladh *et al.* (1999) is used and since it is based on the channel flow code the implementation is similar.

The solution of the adjoint equations require knowledge about the full state in space and time from the solution of the Navier–Stokes system. This is achieved by saving a large number of velocity fields equidistant in time and interpolating linearly in time when the adjoint equations are solved. This introduces an error, but if the time step between saved field is small enough, we expect a sufficiently accurate approximation. The number of saved velocity fields can become large especially if the time domain is long. An efficient way of reducing the memory requirement is to use a check-pointing technique, see for example Berggren (1998). This decreases the memory requirement at the cost of increased computational time. For the simple test cases presented in this paper check-pointing has not been necessary, but for larger cases, especially simulations requiring high spatial resolution, it will be needed.

4.1.1. *Implementation of control*

The control is implemented as the Fourier coefficients of the v velocity at the wall(s). The control function is discretized in time with a fixed time step that can be used to change the time resolution of the control and there is one set of coefficients for each control time. Linear interpolation is used for the control in times between the discrete control times. The control always starts and ends with zero velocity, and has zero mass flux. The time step in the solution of both the forward and adjoint equations is adjusted to be small enough to at least resolve the control in time, even if the time step allowed for numerical stability is larger.

When simulating a spatial boundary layer the control is applied only on Γ_c which extends over the interval (x_1^c, x_2^c) in the chordwise direction. In the code a filtering is added to handle this, and to ensure that the zero mass flux

condition on the control is enforced,

$$\int_{\Gamma_l} v_c \, \mathrm{d}\Gamma = 0. \tag{41}$$

The control is then modified to have zero velocity outside Γ_c,

$$\int_{\Gamma_l} \tilde{\varphi}_l^T \psi_l \, \mathrm{d}\Gamma = \int_{\Gamma_l} (\varphi_l^T \psi_l + c)\chi(x_1^c, x_2^c) \, \mathrm{d}\Gamma = 0 \tag{42}$$

which yields,

$$c = -\frac{\displaystyle\int_{\Gamma_l} \varphi_l^T \psi_l \, \chi(x_1^c, x_2^c) \, \mathrm{d}\Gamma}{\displaystyle\int_{\Gamma_l} \chi(x_1^c, x_2^c) \, \mathrm{d}\Gamma}, \tag{43}$$

and where $\chi(r_1, r_2) = \chi[r_1, r_2](r)$ is defined as:

$$\chi[r_1, r_2](r) = \begin{cases} 1 & \text{if } r \in (r_1, r_2), \\ 0 & \text{otherwise.} \end{cases} \tag{44}$$

The procedure for modifying the control can be summarized as follows:

$$\hat{\varphi}_l \xrightarrow{\text{inverse FFT}} \varphi_l \xrightarrow{\text{Filtering and mass flux correction}} \tilde{\varphi}_l \xrightarrow{\text{FFT}} \hat{\tilde{\varphi}}_l$$

assuming that we denote the original Fourier space control with $\hat{\varphi}_l$ and the final control in Fourier space with $\hat{\tilde{\varphi}}_l$. This final control constitutes the boundary condition in the simulation when the spatial extent of the control is limited.

4.1.2. *Computing the objective function gradient*

The gradient of the objective function is evaluated from the adjoint pressure on the walls as described in section 3.2. When the adjoint equations are solved, the adjoint pressure on the walls must also be computed simultaneously in the control interval. Since the p_1 and p_3 velocities are available at each time step we can compute the pressure gradients σ_x and σ_z using (40). The corresponding pressure is then computed by integrating these gradients with the constant part of the adjoint pressure set to zero, since it does not enter the gradient computation. The adjoint pressure is then projected onto the basis functions of the control using (22), (23) or (31). In the spatial boundary layer case the gradient (31) is computed in Fourier space, but we should only integrate over Γ_c. The gradient is transformed to physical space and there a step function which cuts out the region Γ_c is applied. This filtering procedure is similar to that for the control. The resulting gradient is then transformed back to Fourier space.

4.2. *Optimization routine*

Optimization is performed with a limited memory quasi-Newton method. The algorithm, L-BFGS-B (Byrd *et al.* (1994)), is available on the Internet (the web-link is given in the reference list next to Byrd *et al.* (1994)) and was downloaded and compiled without modifications. It is an algorithm well suited for large non-linear optimization problems, with or without bounds on the control variables. The BFGS method uses an approximation of the Hessian matrix of the objective function, instead of the full matrix. The algorithm has been shown to work well for many different types of optimization problems. The flow of the optimization process is described in Figure 3. The limited memory BFGS algorithm differs from the standard BFGS algorithm in that it never stores the Hessian matrix. Instead only a certain number of gradient and control updates from earlier optimization iterations are stored. These are then used to build an approximation of the Hessian matrix. Consult Byrd *et al.*

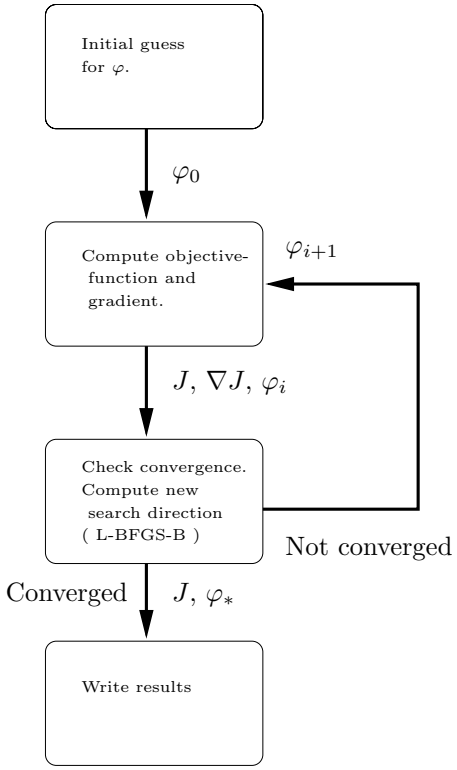

FIGURE 3. The flow in the optimization with L-BFGS-B.

(1994) for details. The inputs to the optimization routine are the control, the gradient of the control and the value of the objective function. A new control is then obtained as output and applied in the next iteration until the convergence

criterion has been met. There are a few different convergence criteria that can be used simultaneously or separately such as the norm of the gradient and the relative reduction of the objective function between iterations.

5. Results

5.1. *Gradient accuracy*

To verify that the implementation is correct as well as that the problem has been formulated correctly, one can check the accuracy of the gradient of the objective function. By perturbing one degree of freedom of the control and computing the resulting change in the objective function the gradient with respect to that degree of freedom can be approximated. Performing this procedure for all degrees of freedom gives the complete objective function gradient. The gradient so computed can then be used to verify that the gradient obtained from the adjoint equation approach is correct. This has been done at different stages of the optimization process for a number of different cases, varying the flow perturbation as well as the initial guess for the control. The accuracy of the gradient direction is quantified by normalizing the two gradients and computing the norm of the difference between them. This difference is less than 1% for all channel and boundary layer flow cases tested when the optimization routine is in the initial iterations. When the gradient accuracy is computed for solutions close to the optimal solution, the accuracy is degraded and the error can be as large as $10\% - 20\%$. This degraded accuracy slows down the convergence of the optimization routine and makes it difficult to reach the true optimal solution.

5.2. *Control of oblique transition in channel flow*

As a first test case, we study the oblique transition scenario. Oblique waves are introduced in the flow, where they grow and induce streamwise vortices. The vortices then produce streamwise streaks that grow until they finally break down and transition occurs. The threshold energies for this type of bypass transition are studied in Reddy *et al.* (1998). The initial stage of this scenario is the growth of oblique waves. If the amplitude is low, this is all that happens before the flow returns to the laminar state. With a higher amplitude, the oblique waves induce enough streamwise vorticity to generate streaks. The streaks grow to a much higher amplitude than the oblique waves. If the initial disturbance is large enough, we get transition to turbulence.

Testing the optimal control on this scenario is done at three different stages and with different time resolution. First control is applied at the very beginning where only the oblique waves are present, secondly the control is applied in the beginning of the streak growth, where both streaks and oblique waves are present. The last case application of the control to the growing streaks. The results in this section were previously reported in Högberg *et al.* (2000).

Five different simulations are performed using the same initial condition. The objective is to minimize the integral of the deviation from the laminar

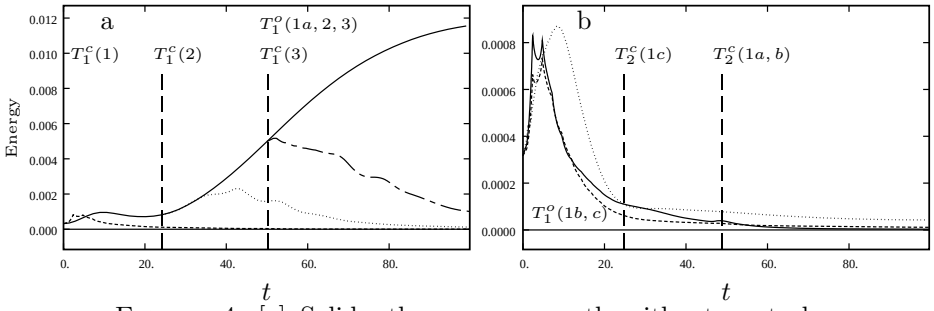

FIGURE 4. [a] Solid: the energy growth without control ; dashed: case 1a ; dotted : case 2 ; dash-dot: case 3. [b] solid: case 1a ; dashed: case 1b ; dotted: case 1c.

flow profile from time T_1^o to $T_2^o = 100$. The Reynolds number is 1500 and the box size is $2\pi \times 2 \times 2\pi$ in x, y, z. In case 1a,b,c the control is applied from time $T_1^c = 0$ until $T_2^c = 50$ in a,b and $T_2^c = 25$ in c. The objective function is measured from $T_1^o = 50$ in case 1a and from $T_1^o = 0$ in cases 1b and 1c. For cases 2 and 3 the control is applied from $T_1^c = 25$ and $T_1^c = 50$ respectively, and the objective function from $T_1^o = 50$. The resulting control velocity in all cases is of the order 2% of the centerline velocity. The reduction of the gradient norm is about three orders of magnitude after 10-15 optimization iterations.

The energy evolution of the controlled flows is shown in Figure 4a. The growth of the oblique waves is efficiently hindered by the control formulation in 1a,b,c and the growth of streaks is eliminated also in cases 2 and 3. In case 2 the control is applied during the formation of the streaks. Initially the energy is allowed to grow but then the growth is hindered by the control and energy decays as. In case 3 the streaks have formed and are growing when control is applied.

In Figure 4b the differences between the controlled flows in cases 1a,b and c are shown. In case 1a the energy is not penalized by the objective function initially as it is in 1b, and this results in lower energy after $t = 50$ than in case 1b. A higher temporal resolution of the control is applied during a shorter time in case 1c. The result is a smoother energy curve but not as low energy at a later time as in the other two cases.

5.3. *Control in a parallel boundary layer flow*

In order to evaluate this type of control strategy for a parallel boundary layer flow we consider an inviscid instability. Inviscid instabilities can exist only if the velocity profile has an inflection point. In a boundary layer flow with a three-dimensional velocity profile, there is always a direction in which such an inflection point exists. In this direction an unstable eigenvalue to the linearized problem was found. The corresponding eigenmode is added to an undisturbed base flow, and the sum is then used as the initial velocity field for the simulations. The base flow is chosen as a Falkner–Skan–Cooke (FSC) flow with the

same parameters as are used in the investigation by Högberg & Henningson (2001) where the Reynolds number is $Re_{\delta_0^*} = 337.9$. The spatial variation of the chordwise mean flow is given through,

$$U_\infty = \left(\frac{x}{x_0} + 1\right)^m,$$

where $x_0 = 354.0$. Furthermore, the cross-flow velocity was $W_\infty = 1.44232$ and $m = 0.34207$. The box dimensions for our simulations are $25.14 \times 20 \times 25.14$ measured in δ^* with a resolution of $4 \times 129 \times 4$ in $x \times y \times z$ respectively. The resolution in the y-direction is chosen fairly large to ensure high accuracy for the y-derivatives needed in the adjoint computation.

For the temporal simulation we use the Falkner–Skan–Cooke flow at $x = 0$. The eigenvalue of the mode used in the simulation is $\omega = (-0.15246 + i0.0382)$, for the parameter choice $\alpha = 0.25$, $\beta = -0.25$. The control is applied from $T_1^c = 0$ to $T_2^c = 150$ and over the entire boundary ($\Gamma_c = \Gamma_l$). The objective function is measured from $T_1^o = 0$ to $T_2^o = 150$ and over the whole spatial domain ($\Omega_o = \Omega$).

Figure 5 shows the disturbance energy growth due to the eigenmode and also the result when the optimal control is applied. As we can see from the figure the exponential energy growth is stopped almost immediately by the control. The first energy peak is mostly due to the energy expenditure to exert control. The maximum magnitude of the control is of the order of 0.02% of the free-stream velocity. The gradient norm is reduced about two orders of

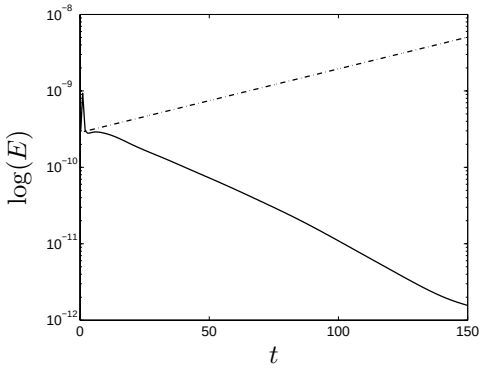

FIGURE 5. Solid: the disturbance energy growth with optimal control ; dash-dot: the disturbance energy growth for temporal FSC flow without control.

magnitude after 5-10 optimization iterations.

5.4. *Control in a spatial boundary layer flow*

A more general flow case to study is when we let the boundary layer grow in the chordwise direction. For this case we have chosen to study a Tollmien-Schlichting (TS) wave in a Blasius boundary layer. The dimensions of the simulation box are $200 \times 20 \times 10$ measured in δ_0^* with a resolution of $96 \times 129 \times 4$ in $x \times y \times z$ respectively. The TS wave is triggered by an oscillating volume force at $x = 10$ which is slightly upstream of branch I, located at $x \approx 40$ where it becomes unstable. The volume forcing does not introduce a pure TS-eigenmode into the flow and this will result in a varying growth of the total energy of the perturbation.

The control is allowed to be active between $T_1^c = 0$ and $T_2^c = 400$ and is located on $\Gamma_c = (20, 70) \times (-5, 5)$. The control is localized in space to give us a region to observe its action downstream of the control area.

The observation time interval is also limited to give the control enough freedom to act initially since we are more interested in the final results. Thus, the objective function is measured from $T_1^o = 380$ to $T_2^o = 400$ over the domain $\Omega_o = (20, 150) \times (0, 20) \times (-5, 5)$ that includes only the physical solution meaning that the fringe region is omitted.

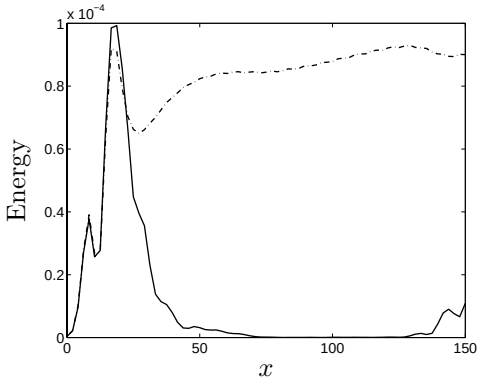

FIGURE 6. Solid: the disturbance energy growth with optimal control ; dash-dot: the disturbance energy growth for a spatial Blasius boundary layer flow without control.

Without the control we can see how the disturbance energy grows in Figure 6, whereas with the optimal control applied on Γ_c the energy growth is efficiently interrupted.

6. Summary and conclusions

First we conclude that optimal control of transition appears to be possible to compute with the approximative discretized adjoint technique used in this work. This was also what the preliminary study by Högberg & Berggren (2000) suggested. In addition, the optimization problem was derived using the primitive

variables velocity and pressure but solved using a velocity–vorticity formulation. This made it easy to implement a solver for the adjoint equations using already developed codes as templates. The adjoint solver thus benefited from the efforts put into making the existing codes computationally efficient.

The optimization routine BFGS by Byrd *et al.* (1994) was found to perform well for the present optimization problems. No modification of the code was necessary.

The test cases for the boundary layer code provide confirmation that we can solve an optimization problem. ¿From the simple parametric study of control of oblique waves in channel flow we can draw a few conclusions.

- The temporal extent of the control appears to be more important than the resolution.
- Allowing a higher energy initially can result in lower energy at a later time.
- It appears that there is enough control authority using blowing and suction on the wall to handle all the different stages of the oblique transition scenario.
- The choice of objective function in terms of time intervals is very important for the performance of the resulting control.

The simple flow cases studied to test the code can now be replaced with more complicated flows. In particular flows where non-linear effects are dominating are of interest, and so are flows with spatial variations in the mean flow profile.

Appendix A. Derivation of gradient for boundary layer

A.1. *The governing equations*

The domain where we solve the governing equations, given $0 < T < +\infty$, is

$$\begin{gathered} \Omega = (-x_l/2, x_l/2) \times (0, y_l) \times (-z_l/2, z_l/2), \\ Q = \Omega \times (0, T). \end{gathered} \tag{45}$$

The boundary of Ω is denoted Γ, and

$$\Gamma_l = \Gamma(y = 0), \quad \Gamma_u = \Gamma(y = y_l), \tag{46}$$

and $\Gamma_c \subset \Gamma_l$ represents the part of the lower boundary where control is applied. For temporal simulations Γ_c coincide with Γ_l.

The governing equations for boundary layer flow are the same as for the channel flow except for an extra term which is added to enforce periodicity of the physical flow in the streamwise direction. This is only needed for spatial simulations.

$$\begin{cases} \dfrac{\partial u}{\partial t} + (u \cdot \nabla)u - \dfrac{1}{Re}\Delta u + \nabla \pi = \lambda(x)(U - u) & \text{in } Q, \\ \nabla \cdot u = 0 & \text{in } Q, \\ u|_{t=0} = u_0, \end{cases} \tag{24}$$

with periodic boundary conditions in the horizontal directions, that is, the x- and z-directions,

$$\begin{aligned} u|_{x=-x_l/2} &= u|_{x=x_l/2}, \\ u|_{z=-z_l/2} &= u|_{z=z_l/2}. \end{aligned} \tag{25}$$

Left to be specified are the conditions in the free-stream and on the wall,

$$\begin{aligned} u|_{y=y_{\text{fst}}} &= U_\infty \quad \left(\text{which is approximated by} \quad \left.\frac{\partial u}{\partial n}\right|_{\Gamma_u} = 0\right), \\ u|_{\Gamma_c} &= n v_c, \\ u|_{\Gamma_l \setminus \Gamma_c} &= 0. \end{aligned} \tag{26}$$

In equation (24), $U = U(x, y)$ is the velocity field that we force the solution towards in the fringe region. Pressure is denoted π and the Reynolds number Re is defined based on the free-stream velocity and the displacement thickness δ^*. The scalar function $\lambda = \lambda(x)$ is nonzero only in the fringe region and is defined as follows:

$$\lambda(x) = \lambda_{\max}\left[S\left(\frac{x - x_{\text{start}}}{\Delta_{\text{rise}}}\right) - S\left(\frac{x - x_{\text{end}}}{\Delta_{\text{fall}}} + 1\right)\right],$$

where $\lambda_{\max}$, x_{start}, x_{end}, Δ_{rise} and Δ_{fall} are parameters used to specify the strength, extent and shape of the fringe forcing. The S-function is defined as,

$$S(r) = \begin{cases} 0 & r \le 0, \\ \dfrac{1}{1 + \exp(1/(1-r) + 1/r)} & 0 < r < 1, \\ 1 & r \ge 1. \end{cases}$$

As for the channel flow case we expand the control v_c in basis functions $\psi_{l,m}$ with zero mass flux, and where $\varphi_{l,m}$ are time dependent coefficients for the basis functions,

$$v_c(x, z, t) = \begin{cases} \varphi_l^T \psi_l = \displaystyle\sum_{m=1}^{M} \varphi_{l,m}(t)\psi_{l,m}(x, z) & \text{in } (T_1^c, T_2^c), \\ 0 & \text{otherwise.} \end{cases} \tag{27}$$

Where we have introduced the control vector φ_l defined as:

$$\varphi_l = (\varphi_{l,1}, \ldots, \varphi_{l,M}).$$

A.2. *The objective function*

We minimize the deviation energy from a given target velocity distribution u_T and add a regularization term including an $\varepsilon > 0$:

$$J(\varphi_l) = \frac{\varepsilon}{2} \int_{T_1^c}^{T_2^c} \int_{\Gamma_c} |v_c|^2 \, \mathrm{d}\Gamma \, \mathrm{d}t + \frac{1}{2} \int_{T_1^o}^{T_2^o} \int_{\Omega_o} |u - u_T|^2 \, \mathrm{d}Q, \tag{28}$$

where (T_1^c, T_2^c) is the control time period and (T_1^o, T_2^o) is the observation time period and Ω_o is the part of the domain Ω where the state of the flow is observed. The control problem can now be defined as:

$$\begin{gathered}\text{Find } \varphi^* \in \mathcal{U}_{\text{ad}} \text{ such that} \\ J(\varphi^*) \leq J(\varphi_l) \quad \forall\ v_c(\varphi_l) \in \mathcal{U}_{\text{ad}},\end{gathered} \tag{47}$$

where φ^* is the optimal control. The set of admissible controls is denoted $\mathcal{U}_{\text{ad}}$ and is a subset of $L^2((T_1^c, T_2^c); \mathbb{R}^M)$.

A.3. *Derivation of the objective function gradient*

We begin by differentiating the objective function (28)

$$\delta J(\varphi_l) = \varepsilon \int_{T_1^c}^{T_2^c} \int_{\Gamma_c} \delta v_c\, v_c \,\mathrm{d}\Gamma\,\mathrm{d}t + \int_{T_1^o}^{T_2^o} \int_{\Omega_o} \delta u \cdot (u - u_T)\,\mathrm{d}Q, \tag{48}$$

where the gradient of J is defined through the directional derivative of J in the $\delta\varphi_l$-direction as done in (4). The differentiated Navier–Stokes equations have the form

$$\begin{cases} \dfrac{\partial \delta u}{\partial t} + (\delta u \cdot \nabla)u + (u \cdot \nabla)\delta u - \dfrac{1}{Re}\Delta \delta u + \nabla \delta \pi = -\lambda(x)\delta u & \text{in } Q, \\ \nabla \cdot \delta u = 0 & \text{in } Q, \\ \delta u|_{t=0} = 0, \end{cases} \tag{49}$$

with the boundary conditions

$$\begin{aligned} \delta u|_{x=-x_l/2} &= \delta u|_{x=x_l/2}, \\ \delta u|_{z=-z_l/2} &= \delta u|_{z=z_l/2}, \\ \delta u|_{y=y_{\text{fst}}} &= 0, \\ \delta u|_{\Gamma_c} &= n\delta v_c, \\ \delta u|_{\Gamma_l \setminus \Gamma_c} &= 0, \end{aligned} \tag{50}$$

where

$$\delta v_c(x,z,t) = \begin{cases} \delta\varphi_l^T \psi_l = \displaystyle\sum_{m=1}^{M} \delta\varphi_{l,m}(t)\psi_{l,m}(x,z) & \text{in } (T_1^c, T_2^c), \\ 0 & \text{otherwise.} \end{cases} \tag{51}$$

Now, let us consider the adjoint variable $p = p(x,y,z,t)$ and the adjoint pressure $\sigma = \sigma(x,y,z,t)$ and require p to satisfy the boundary conditions:

$$\begin{aligned} p|_{x=-x_l/2} &= p|_{x=x_l/2}, \\ p|_{z=-z_l/2} &= p|_{z=z_l/2}, \\ p|_{\Gamma_l} &= 0, \\ p|_{y=y_{\text{fst}}} &= 0. \end{aligned} \tag{52}$$

The boundary condition at $y = y_{\text{fst}}$ can be approximated with the artificial boundary condition

$$\left.\frac{\partial p}{\partial n}\right|_{\Gamma_u} = 0,$$

in the numerical simulations. With a sufficiently high box not only this condition will hold but also p and σ will approach zero.

By multiplying the first equation in (49) with p and then integrating over Q we obtain

$$\begin{aligned}\int_Q p \cdot \Bigg(&\underbrace{\frac{\partial \delta u}{\partial t}}_{1} + \underbrace{(\delta u \cdot \nabla) u}_{2} + \underbrace{(u \cdot \nabla)\delta u}_{3} \\ &\underbrace{-\frac{1}{Re}\Delta \delta u + \nabla \delta \pi}_{4} + \underbrace{\lambda(x)\delta u}_{5} \Bigg) \mathrm{d}Q = 0.\end{aligned} \tag{53}$$

We apply integration by parts in space and time to move the derivatives from u to the adjoint variable p. For clarity we perform this step by step for each term. The first term gives

$$\begin{aligned}\int_Q p \cdot \frac{\partial \delta u}{\partial t}\,\mathrm{d}Q &= \int_\Omega \left(p(T)\cdot\delta u(T) - p(0)\cdot\delta u(0)\right)\mathrm{d}\Omega \\ &\quad - \int_Q \frac{\partial p}{\partial t}\cdot\delta u\,\mathrm{d}Q \\ &= \int_\Omega p(T)\cdot\delta u(T)\,\mathrm{d}\Omega - \int_Q \frac{\partial p}{\partial t}\cdot\delta u\,\mathrm{d}Q,\end{aligned} \tag{54}$$

where we have used the fact that $\delta u(t=0)=0$. Next, we consider the fourth term

$$
\begin{aligned}
&-\frac{1}{Re}\int_Q p\cdot\Delta\delta u\,\mathrm{d}Q+\int_Q p\cdot\nabla\delta\pi\,\mathrm{d}Q\\
&\quad=-\frac{1}{Re}\int_0^T\left[\int_\Gamma p\cdot\frac{\partial\delta u}{\partial n}\,\mathrm{d}\Gamma+\int_\Omega\nabla p:\nabla\delta u\,\mathrm{d}\Omega\right]\mathrm{d}t\\
&\qquad+\int_0^T\left[\int_\Gamma p\cdot n\,\delta\pi\,\mathrm{d}\Gamma\,\mathrm{d}t-\int_\Omega\nabla\cdot p\,\delta\pi\,\mathrm{d}\Omega\right]\mathrm{d}t\\
&\quad=\int_0^T\int_{\Gamma_u} p\cdot\left(n\,\delta\pi-\frac{1}{Re}\frac{\partial\delta u}{\partial n}\right)\mathrm{d}\Gamma\,\mathrm{d}t+\frac{1}{Re}\int_0^T\int_\Gamma\frac{\partial p}{\partial n}\cdot\delta u\,\mathrm{d}\Gamma\,\mathrm{d}t\\
&\qquad-\frac{1}{Re}\int_Q\Delta p\cdot\delta u\,\mathrm{d}Q-\int_Q\nabla\cdot p\,\delta\pi\,\mathrm{d}Q\\
&\quad=\frac{1}{Re}\int_0^T\int_{\Gamma_u}\frac{\partial p}{\partial n}\cdot\delta u\,\mathrm{d}\Gamma\,\mathrm{d}t+\frac{1}{Re}\int_{T_1^c}^{T_2^c}\left[\delta\varphi_l^T\int_{\Gamma_l}\psi_l\nabla p_2\cdot n\,\mathrm{d}\Gamma\right]\mathrm{d}t\\
&\qquad-\frac{1}{Re}\int_Q\Delta p\cdot\delta u\,\mathrm{d}Q-\int_Q\nabla\cdot p\,\delta\pi\,\mathrm{d}Q,
\end{aligned}
\tag{55}
$$

where $p=(p_1,p_2,p_3)$. In the second equality we used the boundary condition (30) for p at $y=0$ and enforced symmetry. In the third equality the condition for δu at $y=0$ in (50) was used. We also assumed that p goes to zero at the artificial boundary $y=y_l$. The : denotes a complete contraction defined as in (12).

The next term to rewrite, in relation (53), is the second term

$$
\int_Q p\cdot(\delta u\cdot\nabla)u\,\mathrm{d}Q=\int_Q(\nabla u)^T p\cdot\delta u\,\mathrm{d}Q. \tag{56}
$$

Finally, we rewrite the third term in (53)

$$\begin{aligned}
&\int_Q p\cdot(u\cdot\nabla)\delta u\,\mathrm{d}Q\\
&\quad=\int_0^T\!\!\int_\Gamma (p\cdot\delta u)(n\cdot u)\,\mathrm{d}\Gamma\,\mathrm{d}t\\
&\qquad-\int_Q (p\cdot\delta u)(\nabla\cdot u)\,\mathrm{d}Q-\int_Q (u\cdot\nabla)p\cdot\delta u\,\mathrm{d}Q\\
&\quad=\int_0^T\!\!\int_{\Gamma_u} (p\cdot\delta u)(n\cdot u)\,\mathrm{d}\Gamma\,\mathrm{d}t-\int_Q (u\cdot\nabla)p\cdot\delta u\,\mathrm{d}Q,
\end{aligned}\tag{57}$$

where we have used the continuity condition on u and the boundary conditions (30) for p. The fifth term needs no rewriting.

Substituting (54), (55), (56) and (57) into (53) yields

$$\begin{aligned}
&\int_\Omega p(T)\cdot\delta u(T)\,\mathrm{d}\Omega+\frac{1}{Re}\int_{T_1^c}^{T_2^c}\left[\delta\varphi_l^T\int_{\Gamma_l}\psi_l\nabla p_2\cdot n\,\mathrm{d}\Gamma\right]\mathrm{d}t\\
&\quad+\int_Q \delta u\cdot\left(-\frac{\partial p}{\partial t}+(\nabla u)^T p-(u\cdot\nabla)p-\frac{1}{Re}\Delta p+\lambda(x)p\right)\mathrm{d}Q\\
&\quad-\int_Q \delta\pi\nabla\cdot p\,\mathrm{d}Q+\frac{1}{Re}\int_0^T\!\!\int_{\Gamma_u}\frac{\partial p}{\partial n}\cdot\delta u\,\mathrm{d}\Gamma\,\mathrm{d}t\\
&\quad+\int_0^T\!\!\int_{\Gamma_u}(n\cdot u)(p\cdot\delta u)\,\mathrm{d}\Gamma\,\mathrm{d}t=0.
\end{aligned}\tag{58}$$

Now, require p to satisfy the adjoint equations:

$$\begin{cases}
-\dfrac{\partial p}{\partial t}+(\nabla u)^T p-(u\cdot\nabla)p\\
\quad-\dfrac{1}{Re}\Delta p+\lambda(x)p+\nabla\sigma=\begin{cases}u-u_T & \text{in } (T_1^o,T_2^o)\times\Omega_o\\ 0 & \text{otherwise}\end{cases} & \text{in } Q,\\
\nabla\cdot p=0 & \text{in } Q,\\
p|_{t=T}=0,
\end{cases}\tag{29}$$

with the boundary conditions (30). With these assumptions equation (58) becomes

$$\begin{aligned}\int_{T_1^o}^{T_2^o}\int_{\Omega_o} \delta u \cdot (u - u_T)\,\mathrm{d}Q - \int_Q \delta u \cdot \nabla\sigma\,\mathrm{d}Q \\ + \frac{1}{Re}\int_0^T\int_{\Gamma_u} \frac{\partial p}{\partial n}\cdot\delta u\,\mathrm{d}\Gamma\,\mathrm{d}t + \int_0^T\int_{\Gamma_u}(n\cdot u)(p\cdot\delta u)\,\mathrm{d}\Gamma\,\mathrm{d}t = 0,\end{aligned} \tag{59}$$

since p and $\partial p_2/\partial n$ is zero on the boundary $y = 0$ due to the no-slip and continuity conditions. The second term in (59) can be rewritten

$$\begin{aligned}-\int_Q \delta u\cdot\nabla\sigma\,\mathrm{d}Q &= -\int_0^T\int_\Gamma \delta u\cdot n\,\sigma\,\mathrm{d}\Gamma\,\mathrm{d}t + \int_Q \nabla\cdot\delta u\,\sigma\,\mathrm{d}Q \\ &= -\int_0^T\int_\Gamma \delta u\cdot n\,\sigma\,\mathrm{d}\Gamma\,\mathrm{d}t,\end{aligned} \tag{60}$$

since $\nabla\cdot\delta u = 0$. The final step is now to substitute the terms involving δu. When that is done the second term in the perturbed objective function (48) can be replaced with terms involving $\delta\varphi$. Since δu is known on parts of the boundary we can proceed as follows

$$\begin{aligned}-\int_0^T\int_\Gamma \delta u\cdot n\,\sigma\,\mathrm{d}\Gamma\,\mathrm{d}t \\ = -\int_0^T\int_{\Gamma_u}\delta u\cdot n\,\sigma\,\mathrm{d}\Gamma\,\mathrm{d}t + \int_{T_1^c}^{T_2^c}\left[\delta\varphi_l^T\int_{\Gamma_c}\psi_l\sigma\,\mathrm{d}\Gamma\right]\mathrm{d}t.\end{aligned} \tag{61}$$

Combining equation (60) and (61) and inserting that into (59) yield

$$\begin{aligned}\int_{T_1^o}^{T_2^o}\int_{\Omega_o}\delta u\cdot(u-u_T)\,\mathrm{d}Q + \int_0^T\int_{\Gamma_u}\delta u\cdot\left(\frac{1}{Re}\frac{\partial p}{\partial n} - \sigma n + (n\cdot u)p\right)\mathrm{d}\Gamma\,\mathrm{d}t \\ + \int_{T_1^c}^{T_2^c}\left[\delta\varphi_l^T\int_{\Gamma_c}\psi_l\sigma\,\mathrm{d}\Gamma\right]\mathrm{d}t = 0.\end{aligned} \tag{62}$$

Applying the fourth boundary condition (30) for p together with the assumption that also $p = 0$ and $\sigma = 0$ (see the beginning of the section) at $y = y_l$ we get

$$\int_{T_1^o}^{T_2^o} \int_{\Omega_o} \delta u \cdot (u - u_T) \, \mathrm{d}Q = - \int_{T_1^c}^{T_2^c} \left[\delta \varphi_l^T \int_{\Gamma_c} \psi_l \sigma \, \mathrm{d}\Gamma \right] \mathrm{d}t. \tag{63}$$

Remains only to substitute (63) into (48) which yields

$$\delta J(\varphi_l) = \int_{T_1^c}^{T_2^c} \delta \varphi_l^T \int_{\Gamma_c} \psi_l \left(\varepsilon \varphi_l^T \psi_l - \sigma \right) \, \mathrm{d}\Gamma \, \mathrm{d}t \tag{64}$$

where the gradient of the objective function can be identified as:

$$\frac{\partial J}{\partial \varphi_l} = \int_{\Gamma_c} \psi_l \left(\varepsilon \varphi_l^T \psi_l - \sigma \right) \, \mathrm{d}\Gamma. \tag{31}$$

This is exactly the same expression for the gradient as for the channel flow case, equation (22) and (23), except that this gradient is restricted to information from Γ_c.

References

Berggren, M. 1998 Numerical solution of a flow-control problem: vorticity reduction by dynamic boundary action. *SIAM J. Sci. Comp.* **19** (3), 829–860.

Bewley, T. R., Moin, P. & Temam, R. 2001 DNS-based predictive control of turbulence: an optimal benchmark for feedback algorithms. *J. Fluid Mech.* **447**, 179–225.

Byrd, R. H., Peihuang, L., Nocedal, J. & Zhu, C. 1994 A limited memory algorithm for bound constrained optimization. Technical Report NAM-08. EECS Department, Northwestern University, `http://www.netlib.org/toms/778`.

Canuto, C., Hussaini, M. Y., Quarteroni, A. & Zang, T. A. 1988 *Spectral Methods in Fluids Dynamics*. Springer.

Collis, S., Chang, Y., Kellogg, S. & Prabhu, R. D. 2000 Large eddy simulation and turbulence control. AIAA Paper 2000–2564.

Glowinski, R. & He, J. 1998 On shape optimization and related issues. In *Computational Methods for Optimal Design and Control* (eds. J. Borggaard, J. Burns, E. Cliff & S. Schreck), pp. 151–179. Birkhäuser, Boston.

Gunzburger, M. D., ed. 1995 *Flow Control*. Springer-Verlag.

Gunzburger, M. D. 1998 Sensitivities in computational methods for optimal flow control. In *Computational Methods for Optimal Design and Control* (eds. J. Borggaard, J. Burns, E. Cliff & S. Schreck), pp. 197–236. Birkhäuser, Boston.

Hinze, M. & Kunish, K. 2000 Three control methods for time dependent fluid flow. *Flow, Turbulence and Combustion* **65** (3/4), 273–298.

Högberg, M. & Berggren, M. 2000 Numerical investigation of different discretization approaches for optimal control. *Flow, Turbulence and Combustion* **65** (3/4), 299–320.

Högberg, M. & Bewley, T. R. 2001 Spatially-localized convolution kernels for decentralized control and estimation of transition of plane channel flow. *Automatica* Submitted.

Högberg, M. & Henningson, D. S. 2001 Linear optimal control applied to instabilities in spatial boundary layers. *J. Fluid Mech.* Submitted.

Högberg, M., Henningson, D. S. & Berggren, M. 2000 Optimal control of bypass transition. In *Advances in turbulence VIII* (ed. D. C.).

Joslin, R. D., Gunzburger, M. D., Nicolaides, R. A., Erlebacher, G. & Hussaini, M. Y. 1997 A Self-contained, Automated Methodology for Optimal Flow Control Validated for Transition Delay. *AIAA Journal* **35** (5), 816–824.

Kim, J. & Lim, J. 2000 A linear process in wall-bounded turbulent shear flows. *Phys. Fluids* **12** (8), 1885–1888.

Lundbladh, A., Berlin, S., Skote, M., Hildings, C., Choi, J., Kim, J. & Henningson, D. S. 1999 An Efficient Spectral Method for Simulations of Incompressible Flow over a Flat Plate. Technical Report TRITA-MEK 1999:11. Royal Institute of Technology, Department of Mechanics, KTH.

Lundbladh, A., Henningson, D. S. & Johansson, A. 1992 An Efficient Spectral Integration Method for the Solution of the Navier-Stokes Equations. Technical Report FFA TN 1992-28. The Aeronautical Research Institute of Sweden, FFA.

Morkovin, M. V. 1969 The many faces of transition. In *Viscous Drag Reduction* (ed. C. S. Wells). Plenum Press.

Nordström, J., Nordin, N. & Henningson, D. S. 1999 The fringe region technique and the fourier method used in the direct numerical simulation of spatially evolving viscous flows. *SIAM J. Sci. Comp.* **20** (4), 1365–1393.

Reddy, S. C., Schmid, P. J., Baggett, J. S. & Henningson, D. S. 1998 On stability of streamwise streaks and transition thresholds in plane channel flows. *J. Fluid Mech.* **365**, 269–303.

Schmid, P. J. & Henningson, D. S. 2001 *Stability and transition in shear flows*. Springer-Verlag.

Sritharan, S. S., ed. 1998 *Optimal control of viscous flows*. SIAM.

Paper 3

3

Accuracy of gradient computations for aerodynamic shape optimization problems

By Mattias Chevalier* and Martin Berggren*

Applying nonlinear optimization techniques such as quasi-Newton methods to aerodynamic shape optimization problems requires the calculation of gradients of a given objective function. An effective way of calculating such gradients is through the use of the so-called adjoint equations. To achieve fast convergence in the optimization algorithm, accurately computed gradients are needed. In the computation of such gradients the discretization of the problem and the choice of boundary conditions are two important aspects. These issues are studied in the context of shape optimization of a quasi-1D nozzle using physically relevant boundary conditions. Isentropy is enforced at the inlet boundary, and the static pressure is specified at the outlet boundary for subsonic flows. A cell-centered finite-volume discretization with a standard implementation of the boundary conditions is applied, and the corresponding numerical scheme and numerical boundary conditions for the adjoint equations are derived in a fully discrete sense.

Numerical experiments at subsonic and transonic speeds, show that the gradient evaluations are accurate enough to obtain satisfactory convergence of the quasi-Newton algorithm.

1. Introduction

As more and more powerful computers develop, the range of problems possible to solve numerically increases. One class of such problem is aerodynamic shape optimization using the Euler or Navier–Stokes equations as the flow model.

Discretization issues in connection with aerodynamic shape optimization are discussed in this article. A simple model for nozzle flow is the quasi-1D Euler equations, in which the nozzle geometry is represented as a scalar function occurring in the coefficients of the equation. This is a standard model problem for transonic flow sharing many features with more complicated models, but having a known solution in terms of an implicit formula for the Mach number and the area function. An objective (or cost) function is introduced to measure, in a least-square sense, how far from the optimal design we are. To improve

*FFA, The Aeronautical Research Institute of Sweden†.
†Former FFA now sorts under The Swedish Defence Research Agency (FOI) as the Aeronautics Divsion, SE-172 90 Stockholm, Sweden

the geometry, we use optimization methods that utilize the objective function gradient, computed with the aid of the *adjoint equations*.

We will state the adjoint equations, derived from the state equation and objective function using physically relevant boundary conditions. A *quasi-discrete* form of the adjoint equations will also be stated. That is, the precise form of the discretization of the Euler equations as well as the precise way in which the boundary conditions are implemented are taken into account when the adjoint equations are derived. However, the precise form of the coefficients in the artificial dissipation terms is *not* reflected in the adjoint equations.

This approach is just one among several ways of finding the gradient to the objective function. Using finite differences on each of the design variables is another alternative. A third alternative is to compute so-called flow sensitivities by repeatedly solve linearized versions of the equations. These alternatives are easier to implement but are computationally costly. The cost of computing the gradient from the adjoint equations has the advantage of being independent of the number of design variables.

Several authors, such as Iollo *et al.* (1993), Narducci *et al.* (1995), Ibrahim & Oktay (1994), and Cliff *et al.* (1997), have published works on shape optimization for the quasi-one-dimensional nozzle flow. In a very recent article, Giles & Pierce (2001) also derive analytical expressions for solutions to the adjoint equations. Most of these articles concentrate on the particular difficulties that are associated with embedded shocks in the flow. In contrast to this, we limit ourselves to the case of smooth flow when deriving expressions for the gradient of the objective function. This is done to highlight the distinct features of the current investigation: the choice of boundary conditions together with the use of the quasi-discrete form of the adjoint equations.

The article is organized as follows. Section 2 introduces the governing equations and the shape optimization problem. Section 3 describes the numerical treatment of the equations involved. Section 4 presents computational results and is followed by the final discussion of section 5.

2. Theory

2.1. *The shape optimization problem*

The quasi-1D Euler equations for steady flow are (references Hirsch (1990) and Anderson (1990))

$$\mathbf{f}_x + \xi \mathbf{g} = \mathbf{0}, \tag{1}$$

where the following vector notation is introduced

$$\mathbf{f} = \begin{pmatrix} \rho u \\ \rho u^2 + p \\ (\rho e + p)u \end{pmatrix}, \quad \mathbf{g} = \begin{pmatrix} \rho u \\ \rho u^2 \\ (\rho e + p)u \end{pmatrix}. \tag{2}$$

The equation of state,

$$p = (\gamma - 1)\left(\rho e - \rho\frac{u^2}{2}\right), \tag{3}$$

closes the system. Here, x is the streamwise coordinate, ρ is the density, u is the fluid velocity, p is the pressure, e is the total energy per unit mass, and A is the area function. We use $\gamma = 1.4$ (air and standard conditions) for all simulations.

Perhaps the physically most natural choice of inlet boundary conditions for nozzle flow is to specify constant stagnation conditions. When the flow is subsonic at the outlet, we also need to supply a boundary condition there. That is done through the *back pressure*, a given constant static pressure at the outlet. With this choice of boundary conditions, the *state equation* reads

$$\begin{aligned} \mathbf{f}_x + \xi\mathbf{g} &= \mathbf{0} && \text{in } (0,1), \\ p\left(1 + \frac{\gamma-1}{2}M^2\right)^{\gamma/\gamma-1} &= p_s && \text{at } x = 0, \\ T\left(1 + \frac{\gamma-1}{2}M^2\right) &= T_s && \text{at } x = 0, \\ \text{If } M < 1 \quad p &= p_{out} && \text{at } x = 1, \end{aligned} \tag{4}$$

where $\xi = A/A_x$ and where $M = u/c$ is the Mach number; the speed of sound is given by the relation $c^2 = \gamma p/\rho$. The constants p_s and T_s are the given values of the stagnation pressure and stagnation temperature respectively, and p_{out} is the given static pressure at the outlet.

Two independent set of variables, conservative, $\mathbf{w}$, and primitive, $\mathbf{v}$, will be used:

$$\mathbf{w} = \begin{pmatrix} \rho \\ \rho u \\ \rho e \end{pmatrix}, \quad \mathbf{v} = \begin{pmatrix} \rho \\ u \\ p \end{pmatrix}. \tag{5}$$

To exert control on the nozzle flow, the shape of the nozzle will be adjusted. The shape enters the Euler equations through ξ and the most obvious choice of design parameter is ξ. Note however that we could also have used the area, A, and computed ξ from A.

The aim of the optimization is to force the nozzle to mimic a *target* distribution of some flow quantity, in our case, the pressure. To quantify this constraint we introduce an objective function

$$I(\xi) = \frac{1}{2}\int_0^1 (p - p^t)^2\, dx, \tag{6}$$

where p^t is the target pressure distribution and p is the pressure distribution computed from ξ by solving the state equation.

The shape optimization problem corresponds to finding the design ξ, which minimizes the objective function I in (6). Given a target pressure distribution $p^t = p^t(x)$, the problem is

$$\begin{aligned} &\text{Find } \xi^* \in \mathcal{U}_{\text{ad}} \text{ such that} \\ &I(\xi^*) \leq I(\xi) \quad \forall \xi \in \mathcal{U}_{\text{ad}}. \end{aligned} \tag{7}$$

The set of *admissible designs* is denoted $\mathcal{U}_{\text{ad}}$ and is a subset of bounded functions on $[0,1]$. That choice for $\mathcal{U}_{\text{ad}}$ leads to a well-posed problem for the Euler equations. Cliff *et al.* (1997, § 3) give an example of a closed and convex set of this kind.

2.2. *The gradient*

Most minimization algorithms, such as steepest descent, conjugate-gradient, and (quasi-)Newton methods, utilize gradient information. The gradient ∇I of the objective function (6) is defined through taking the directional derivative in the $\delta\xi$ direction:

$$\delta I = \langle \nabla I, \delta\xi \rangle = \lim_{s \to 0} \left| \frac{I(\xi + s\delta\xi) - I(\xi)}{s} \right|, \tag{8}$$

where $\delta\xi$ is an arbitrary variation of the shape. To supply gradient information to a quasi-Newton algorithm, we use the adjoint equation approach.

In Chevalier & Berggren (2000) we derive, by use of standard perturbation analysis applied on the objective function (6) and the state equation (4), an expression for the gradient in terms of the solution to an auxiliary problem, the adjoint equations. Here we only state the final expressions for the gradient and the adjoint equations for subsonic in- and outlet conditions:

$$\nabla I(\xi) = \psi^T \mathbf{g} \quad \text{in } L^2(0,1), \tag{9}$$

where ψ is the solution to the adjoint equations

$$\begin{aligned} -\mathbf{J}^T \psi_x + \mathbf{K}^T \psi\xi + \theta(p - p^t) &= \mathbf{0}, \quad \text{in } (0,1), \\ \mathbf{l}^T \widetilde{\mathbf{J}}^T \psi &= 0, \quad \text{at } x = 0, \\ \begin{pmatrix} \mathbf{j}_1^T \\ \mathbf{j}_2^T \end{pmatrix} \psi &= \mathbf{0}, \quad \text{at } x = 1. \end{aligned} \tag{10}$$

Here, $\mathbf{l}$ is a vector consisting of data computed from flow quantities on the boundary and total quantities assuming isentropic process. The vector θ is the pressure differentiated with respect to $\mathbf{w}$,

$$\theta = \left(\frac{\partial p}{\partial \mathbf{w}} \right)^T.$$

The matrices $\mathbf{J}$, $\mathbf{K}$, and $\widetilde{\mathbf{J}}$ are defined as

$$\mathbf{J} = \frac{\partial \mathbf{f}}{\partial \mathbf{w}}, \quad \mathbf{K} = \frac{\partial \mathbf{g}}{\partial \mathbf{w}}, \quad \widetilde{\mathbf{J}} = \frac{\partial \mathbf{f}}{\partial \mathbf{v}},$$

and $\mathbf{j}_1$, $\mathbf{j}_2$, and $\mathbf{j}_3$ are the column vectors of $\widetilde{\mathbf{J}}$.

Note that in the case of subsonic in- and outlet conditions, the Euler equations have two downstream and one upstream characteristics. For the adjoint equations we have the opposite situation: one downstream and two upstream characteristics due to the negative sign on the Jacobian. This is consistent with the boundary conditions in (10); there are *two* conditions supplied at $x = 1$ and *one* at $x = 0$.

This all summarizes into the following procedure to compute the gradient of I:

1. Solve the state equation (4) given a design ξ.
2. Solve the adjoint equations (10) using the solution obtained above.
3. Compute the gradient from expression (9).

Note that to compute the gradient we basically have to solve only two equally expensive, measured in computer time, systems of equations regardless of how many design parameters we are using.

3. Discretization

A cell-centered finite-volume scheme is applied for the spatial discretization. The step size is constant and denoted $\Delta x = 1/N_x$ where N_x is the number of cells in the domain. The stationary problem is solved by marching the corresponding non-stationary problem to steady state using a five step Runge–Kutta scheme.

The solution vectors, for the whole domain, for conservative and primitive variables are denoted $\{\mathbf{w}_i\}_{i=1}^{N_x}$ and $\{\mathbf{v}_i\}_{i=1}^{N_x}$, respectively. We also define

$$\begin{aligned} \mathbf{f}_i &= \mathbf{f}(\mathbf{w}_i), \\ \mathbf{f}_{i\pm1/2} &= \frac{1}{2}(\mathbf{f}_i + \mathbf{f}_{i\pm1}), \\ \mathbf{g}_i &= \mathbf{g}(\mathbf{w}_i), \end{aligned} \tag{11}$$

where $\mathbf{f}$ and $\mathbf{g}$ are the functions of (2). Integer index i denotes cell-centered values and $i \pm 1/2$ denotes node-centered values.

The discrete state equation is

$$\begin{aligned} \frac{\mathbf{f}_{i+1/2} - \mathbf{f}_{i-1/2}}{\Delta x} + \xi_i \mathbf{g}_i &= \mathbf{d} \quad i = 1, ..., N_x, \\ \begin{pmatrix} \rho_0 \\ u_0 \\ p_0 \end{pmatrix} &= \begin{pmatrix} 2\rho_{1/2} - \rho_1 \\ 2u_{1/2} - u_1 \\ 2p_{1/2} - p_1 \end{pmatrix}, \\ \begin{pmatrix} \rho_{N_x+1} \\ u_{N_x+1} \\ p_{N_x+1} \end{pmatrix} &= \begin{pmatrix} \rho_{N_x} \\ u_{N_x} \\ 2p_{out} - p_{N_x} \end{pmatrix}, \end{aligned} \tag{12}$$

where the vector $\xi_h = \{\xi_i\}_{i=1}^{N_x}$ now is our design variable.

Data for the boundary conditions are supplied through the back pressure p_{out} and through $\rho_{1/2}$ and $p_{1/2}$, which are computed from the isentropic assumptions:

$$\rho_{1/2}\left(1+\frac{\gamma-1}{2}M_1^2\right)^{1/\gamma-1}=\rho_s, \tag{13}$$

$$p_{1/2}\left(1+\frac{\gamma-1}{2}M_1^2\right)^{\gamma/\gamma-1}=p_s, \tag{14}$$

where ρ_s and p_s are the given stagnation density and pressure respectively. The symbol $\mathbf{d}$ on the right-hand side of equation (12) represents artificial dissipation which is needed to stabilize central schemes of this kind. We use the Jameson-style combined second- and fourth-order dissipation.

Solving equation (12), we obtain grid functions like the pressure p_i, $i = 1,\dots,N_x$. Therefore, it is reasonable to approximate the objective function (6) with

$$I_h(\xi)=\frac{1}{2}\Delta x\sum_{i=1}^{N_x}(p_i(\xi)-p_i^t)^2, \tag{15}$$

where $\{p_i\}_{i=1}^{N_x}$ is obtained from the finite-volume solution below and $p_i^t \approx p^t((i-1/2)\Delta x)$ approximates the target pressure.

The discrete counterpart to optimization problem (7) is

$$\begin{gathered}\text{Find } \xi_i^* \in \mathcal{U}_{\text{ad}},\ i=1,\dots,N_x, \text{ such that}\\ I(\{\xi_i^*\}_{i=1}^{N_x}) \le I(\{\xi_i\}_{i=1}^{N_x}) \quad \forall \xi_i \in \mathcal{U}_{\text{ad}}.\end{gathered} \tag{16}$$

3.1. *Gradient computations in the discrete case*

One approach to compute the objective-function gradient is to directly discretize the adjoint equations (10) and the gradient expression (9). However, once discretizations of the Euler equations and the objective function are selected, this implicitly *defines* the *discrete* adjoint equations from which we obtain the expression for the exact gradient of the discretized objective function. This "discrete" adjoint equation may not coincide with a straight-forward discretization of equation (10), particularly not in the implementation of the boundary conditions. Using this discrete gradient minimizes numerical errors in the gradient directions. This may be important since highly accurate gradient directions are typically needed in the quasi-Newton algorithm. However, note that artificial dissipation needs to be added in the adjoint equation for stability and these effects are not taken into account in the derivation.

The discretized equations are derived in detail in Chevalier & Berggren (2000); here we merely state the results. The discrete gradient is

$$\nabla I_h = \Delta x\{\ \psi_i^T \mathbf{g}_i\}_{i=1}^{N_x}, \tag{17}$$

where $\{\ \psi_i\}_{i=1}^{N_x}$ is the solution to the *discrete* adjoint equations

$$\begin{aligned} -\mathbf{J}_i^T \frac{(\ \psi_{i+1} - \ \psi_{i-1})}{2\Delta x} + \xi_i \mathbf{K}_i^T\ \psi_i &= -\ \theta_i (p_i - p_i^t), \\ \mathcal{T}_l\ \psi_0 &= \mathcal{M}_l\ \psi_1, \\ \mathcal{T}_r\ \psi_{N_x+1} &= \mathcal{M}_r\ \psi_{N_x}, \end{aligned} \tag{18}$$

where $i = 1, \ldots, N_x$. The matrices $\mathcal{T}$ and $\mathcal{M}$, defined and derived in Chevalier & Berggren (2000), consist of surprisingly complicated algebraic combinations of flow data at and around the boundaries.

4. Numerical experiments

For the optimization we used the limited-memory quasi-Newton algorithm of Byrd *et al.* (1994), publicly available at `Netlib/toms/778`. Two flow cases are considered, defined by the boundary data in Table 1. These correspond to a fully subsonic and a shock-free transonic case, respectively, using the area function of Figure 1. This particular area function is obtained from a cubic polynomial in $\xi = A/A_x$ using the coefficients in the second column of Table 2. A 200 grid-point mesh is used in all reported experiments.

TABLE 1. Boundary data for the simulated flow types. All quantities are given in SI-units.

Flow	p_s	T_s	ρ_s	p_{out}
Subsonic	200000	300	2.32	174488
Transonic	200000	300	2.32	51159

TABLE 2. Initial and final values of the polynomial coefficients α defining ξ. Here, k denotes the degree of corresponding monomial.

k	Initial α	Target α
0	-0.9474	-0.8574
1	1.1376	1.2376
2	1.7380	1.5980
3	-1.4525	-1.3525

As a first test, we define a target pressure from solving the Euler equation with the area function of Figure 1 and the subsonic data of Table 1. Then the coefficients in the polynomial defining ξ are perturbed (Table 2), and we attempt to recover the target area function by solving the optimization problem (16). This problem is solved using two different parameterizations of the design variable ξ: (i) the coefficients in a cubic polynomials, and (ii) the value of ξ at each grid point. The dimension of the design space is 4 in the first case and 200 in the second. Note that the computational effort needed for

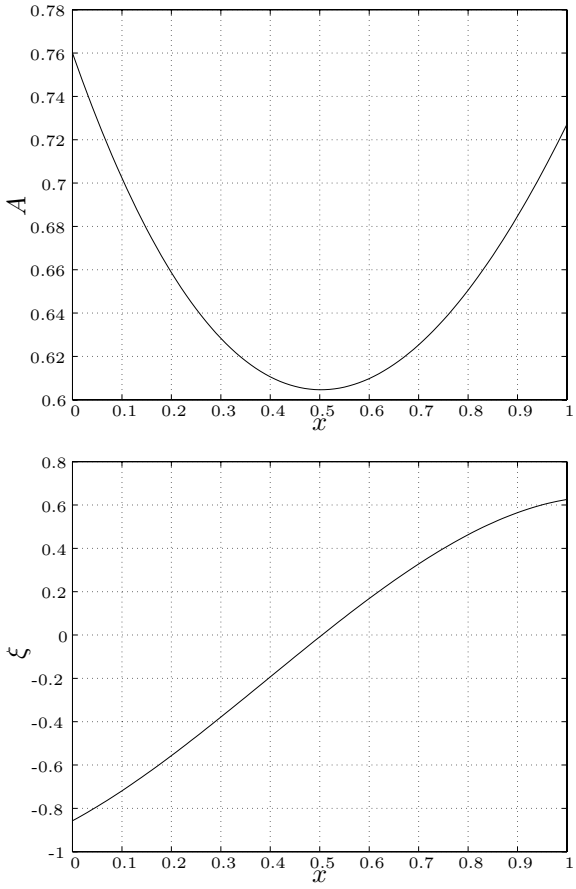

FIGURE 1. Target functions for the area (upper) and ξ (lower).

each quasi-Newton iteration is essentially the same in the two cases, since the adjoint-equation approach is used.

Figure 2 shows the value of the objective function and the norm of the gradient versus iteration number. The convergence behavior for the two different parameterizations of the design are similar for about the 25 first iterations, after which the 4-degrees-of-freedom case appears to enter a region of superlinear convergence for the quasi-Newton method. Figure 3 compares the pressure distribution using the different parameterizations at a few stages in the optimization.

The second test is the same as the first, except that the transonic boundary data of Table 1 are used instead. Figure 4 shows the convergence behavior for the different parameterizations and Figure 5 compares the pressure distributions at different stages in the optimization. The convergence behavior is

similar to the subsonic case, but the superlinear convergence appears later, after about 35 iterations.

The tests above may give the impression that parameterizing with low-order polynomials is better than using many degrees of freedom for the design variables. That this is not at all the case in general is demonstrated in the next test. Note that the cases above use target pressures that are *reachable* by a cubic ξ, that is, one particular cubic yields exactly the target pressure. (This means also that the objective function is zero at the optimum.) In a third test, we picked a target pressure distribution which is (most likely) not reachable by any ξ, cubic or not. Figure 7 shows the convergence behavior when using 4 and 200 design variables, respectively. Note that both the convergence behavior and the final value of the objective function is better when using a higher degree of the design space. Figure 8 depicts the target pressure and the pressure distribution at different stages in the optimization.

In a last test case, using data from the first test problem above with 200 design variables, we test the influence of the boundary conditions at $x = 0$ for the adjoint equation. We compare the use of the "exact" form (18), derived by exact transposition of corresponding boundary conditions of equation (12) with one implementation in which the boundary condition at $x = 0$ in equation (10) are supplemented with "numerical" boundary conditions: extrapolation of two of the variables in ψ. From Figure 6, we see that the difference in the convergence between using these approaches is surprisingly small, considering the elements of arbitrariness in the second approach (which variables should be extrapolated, e.g.?). Inaccuracies in the gradient direction will certainly be introduced in the second approach. That this does not degrade the convergence rate more than indicated in Figure 6 somewhat contradicts the experience of the authors from other studies (Högberg *et al.* (1999)), in which the convergence rate of a related optimization problem was sensitive to small inaccuracies introduced in the gradient directions.

There are at least three possible reasons for this. The cases in which we have formerly noted significant effects on the accuracy of the gradient by changes in the implementation have all concerned parabolic or elliptic state equations. The objective function in such cases is often quite insensitive to small changes in the control (or design), which means that precise gradient information is crucial since the objective function will hardly decrease otherwise. In the present case, the state equation is hyperbolic, and the objective function is quite sensitive to small changes in the design. Thus, precise gradient information may be less important in this case, since even a slightly off gradient direction may greatly reduce the objective function.

A second reason could be that other inaccuracies dominate. For instance, we do not consider the exact form of the artificial dissipation of the state equation when deriving the adjoint equations.

A third reason could be effects of the zeroth-order extrapolation used for the Mach number in defining the pressure and density at $x = 0$ (expression (14)).

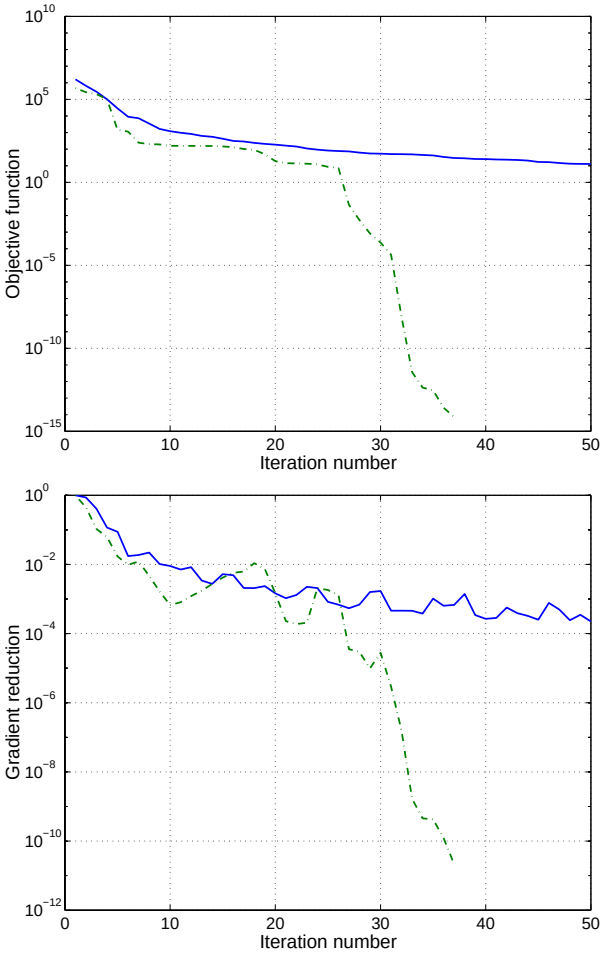

FIGURE 2. The objective function (upper) and the gradient (lower) as functions of iteration number for both polynomial (green/dash-dotted) and full (blue/solid) description of ξ for subsonic flow.

This affects the solution in the form of small, local "kinks" close to $x = 0$. We observed no spread of these disturbances downstream in the solution to the state equation. However, since the boundary conditions for the adjoint equation are derived from the actual boundary conditions used in the state equation, it may well be that the effects on the *adjoint* equations of the zeroth-order extrapolation in the *state* equation is significant. Evidence for this claim is that we noted oscillations in the solution of the adjoint equations originating at the boundary $x = 0$. This could cause an increase of the conditioning of the discrete optimization problem (16) of purely numerical origin.

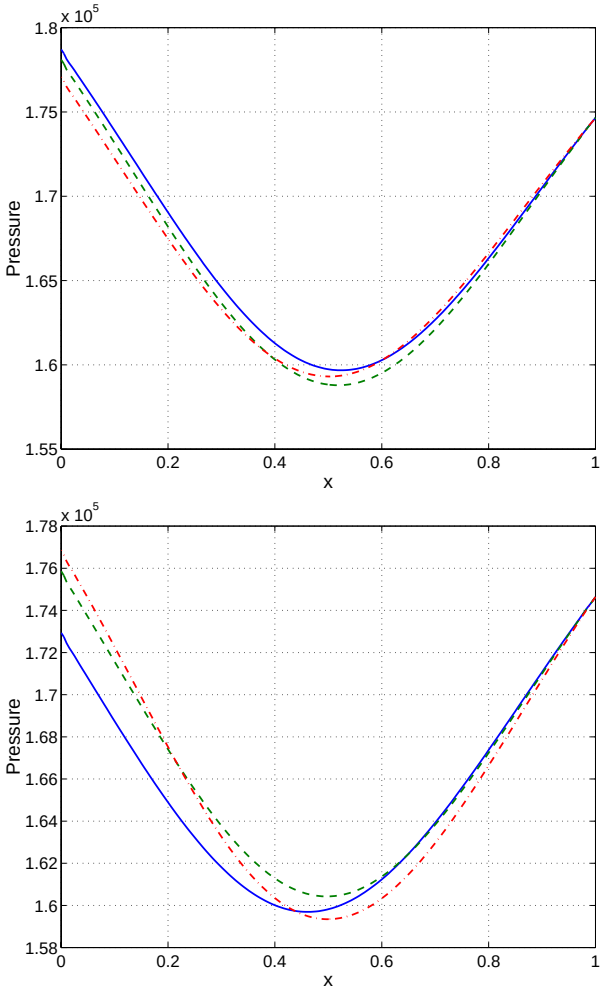

FIGURE 3. Pressure distributions for polynomial (upper) and full (lower) descriptions of ξ at 1 (blue/solid), 3 (green/dashed), and 10 (red/dash-dotted) iterations for subsonic flow.

5. Conclusions and outlook

We have derived, implemented and tested a quasi-discrete form of the adjoint equations to the quasi-1D Euler equations for nozzle flow in order to compute gradients in a shape optimization procedure. Physically relevant boundary conditions are used. For the adjoint equations, we apply corresponding boundary conditions, derived by transposing the exact form in which the boundary conditions for the Euler equations are implemented.

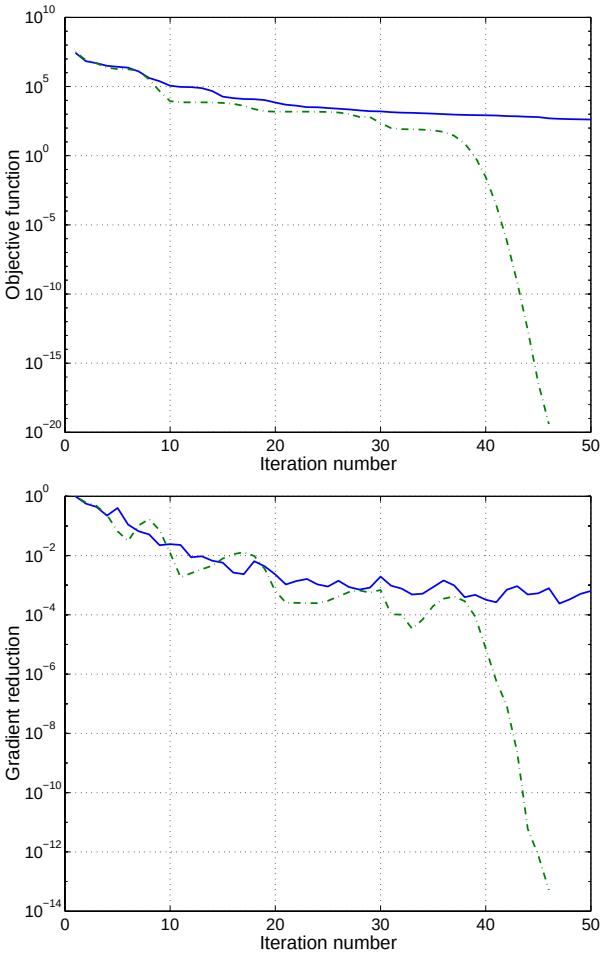

FIGURE 4. The objective function (upper) and the gradient (lower) as functions of iteration number for both polynomial (green/dash-dotted) and full (red/solid) description of ξ for transonic flow.

The gradient computed in this way could be successfully used in an optimization procedure to recover a reachable pressure distribution as well as finding area functions that yield a pressure distribution that well approximates a nonreachable pressure distribution. We demonstrated this in the subsonic as well as the transonic, shock-free regime. Numerical experiments, not reported here, were also performed for cases with embedded shocks. These cases worked surprisingly well, considering that the important effects of the artificial dissipation in the vicinity of the shock were not considered at all in the gradient derivation. However, the convergence rate of the optimization algorithm was

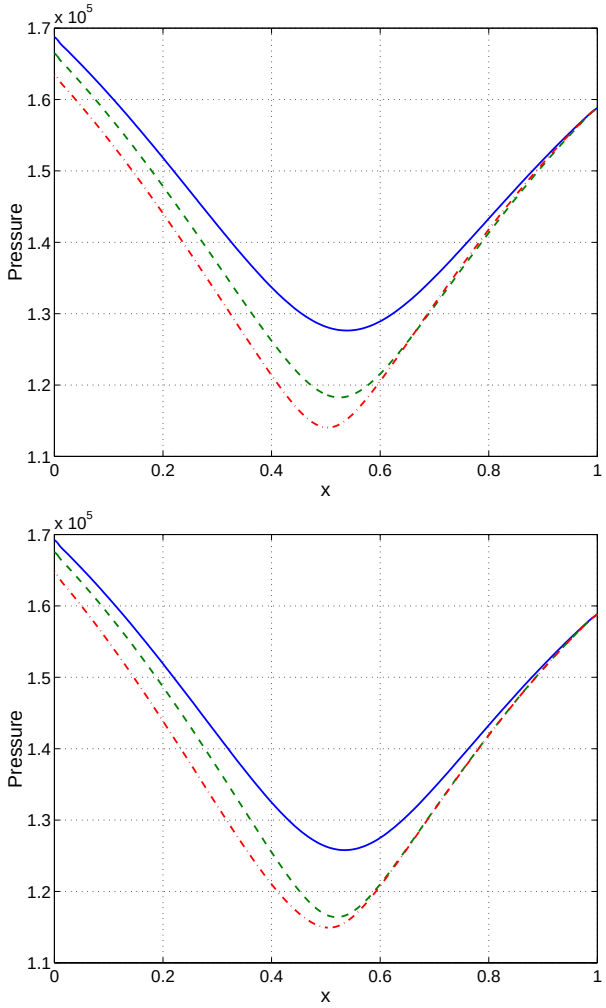

FIGURE 5. Pressure distributions for polynomial (upper) and full (lower) descriptions of ξ at 1 (blue/solid), 3 (green/dashed), and 10 (red/dash-dotted) iterations for transonic flow.

not as good as in the reported cases. To implement a dissipation mechanism in the adjoint equations in a similar "discrete" way as the boundary conditions studied here is an obvious, but nontrivial candidate for a next stage in the development.

As discussed in section 4, we noted some oscillations in the solution to the adjoint equations originating at the boundary $x = 0$. We conjecture that the cause of this is the zeroth-order extrapolation used for the Mach number in the

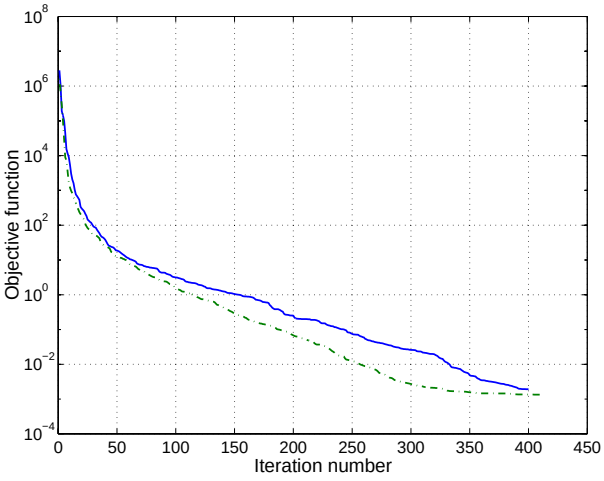

FIGURE 6. The objective function as a function of iteration number for the case when using "exact" boundary conditions (green/dash-dotted) and when using "numerical" boundary conditions (red/solid) for the adjoint equations.

state equation at $x = 0$. Using instead a first-order extrapolation of the Mach number, the local "kinks" in the vicinity of the boundary can be avoided altogether. It would be interesting to see if this also improves the smoothness of the adjoint solution and the conditioning of the optimization problem. However, the derivation of the corresponding adjoint boundary condition is complicated and tedious.

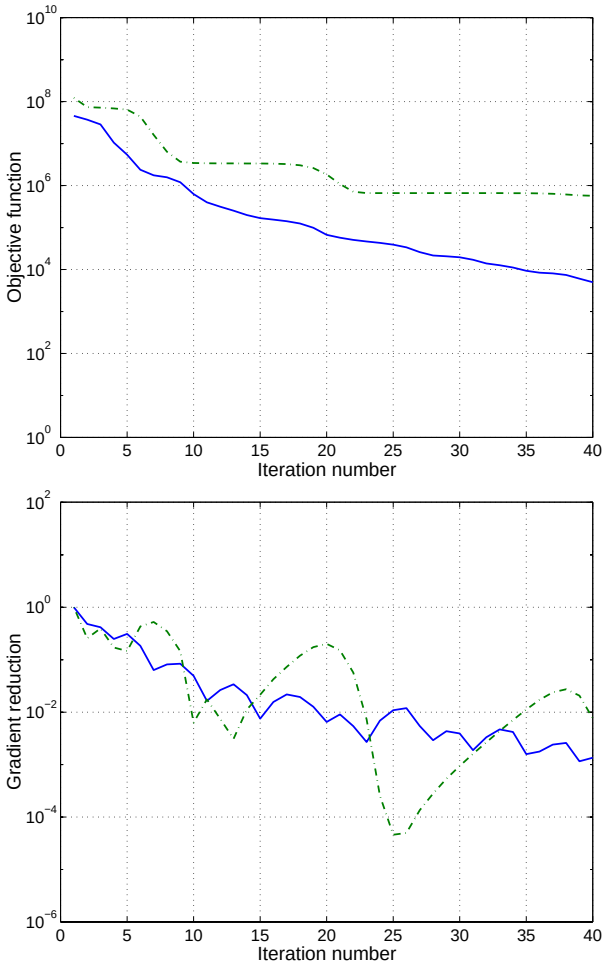

FIGURE 7. The objective function (upper) and the gradient (lower) as functions of iteration number for both polynomial (green/dash-dotted) and full (red/solid) description of ξ for a nonreachable target pressure distribution.

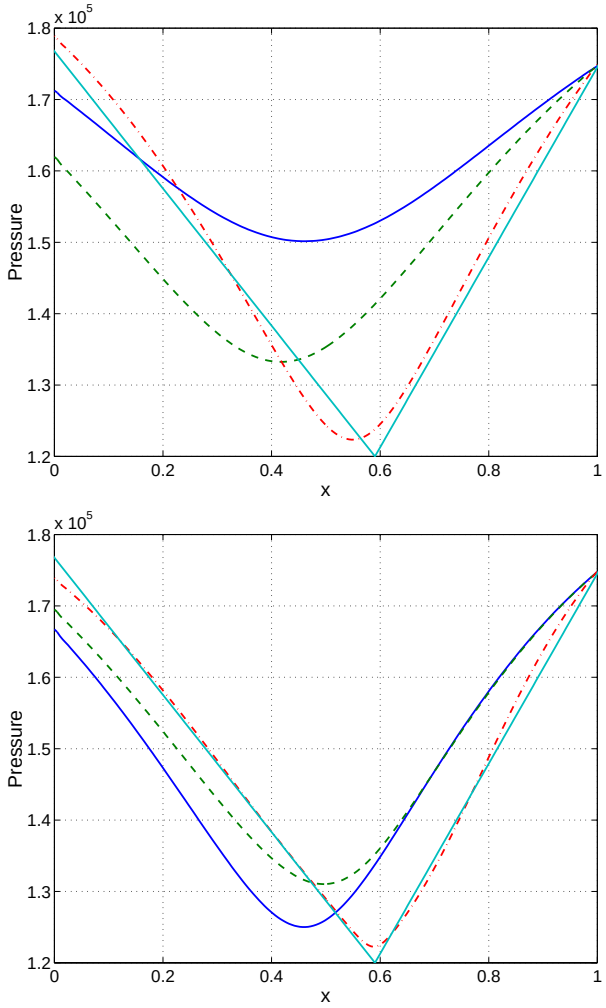

FIGURE 8. Pressure distributions for polynomial (upper) and full (lower) descriptions of ξ at 1 (blue/solid), 3 (green/dashed), and 10 (red/dash-dotted) iterations for a non-reachable target pressure distribution. The target pressure distribution is also plotted (light blue/thin solid).

Acknowledgments

Part of the research was done when the first author was a student for Professor Roland Glowinski which is greatfully acknowledged.

References

Anderson, J. D. 1990 *Modern compressible flow with historical perspective*. Springer-Verlag.

Byrd, R. H., Peihuang, L., Nocedal, J. & Zhu, C. 1994 A limited memory algorithm for bound constrained optimization. Technical Report NAM-08. EECS Department, Northwestern University, `http://www.netlib.org/toms/778`.

Chevalier, M. & Berggren, M. 2000 Accuracy of gradient computations for aerodynamic shape optimization problems. *Tech. Rep.* TN 2000-31. FFA, the Aeronautical Research Institute of Sweden, P. O. Box 11021, S-161 11 Bromma, Sweden.

Cliff, E. M., Heinkenschloss, M. & Shenoy, A. R. 1997 An optimal control problem for flows with discontinuities. *J. Optim. Theory Appl.* **94**, 273–309.

Giles, M. B. & Pierce, N. A. 2001 Analytic adjoint solutions for the quasi-one-dimensional Euler equations. *J. Fluid Mech.* **426**, 327–345.

Hirsch, C. 1990 *Numerical Computation of Internal and External Flows*, , vol. 1 and 2. Wiley.

Högberg, M., Berggren, M. & Henningson, D. S. 1999 Numerical investigation of different discretization approaches for optimal control. *Tech. Rep.* TN 1999-74. FFA, the Aeronautical Research Institute of Sweden, P. O. Box 11021, S-161 11 Bromma, Sweden.

Ibrahim, A. H. & Oktay, B. 1994 Design optimization using variational methods and CFD. AIAA Paper 94–0093.

Iollo, A., Salas, M. D. & Ta'asan, S. 1993 Shape optimization governed by the euler equations using an adjoint method. NASA Contractor Report 191555.

Narducci, R., Grossman, B. & Haftka, R. T. 1995 Sensitivity algorithms for an inverse design problem involving a shock wave. *Inverse Problems in Engineering* **2**, 49–83.